OPEN ACCESS
Freely Available Online

Journal of New Developments in Chemistry
ISSN NO: 2377-2549

Research Article

DOI : 10.14302/issn.2377-2549.jndc-17-1459

FT-IR, FT-Raman, HOMO-LUMO and UV-Visible spectral analysis of E-[N'-(1H-INDOL-3YL) METHYLENE ISONICOTINOHYDRAZIDE]

D.Sumathi[a], H. Saleem[a]*, A. Nathiya[a], N.RameshBabu[b],D.Usha[c]
[a]Department of Physics, Annamalai University, Annamalainagar-608 002, Tamil Nadu, India
[b]Department of Physics, MIET Engineering College, Tiruchirappalli – 620 007, Tamil Nadu, India
[c]Department of Physics, Women's Christian college, Nagercoil – 629 001, Tamil Nadu, India

ABSTRACT

A combined experimental and theoretical study on molecular and vibrational structure of E-[N¢-(1H -indol-3yl) methylene isonicotinohydrazide] (ICINH) had been carried out. The FTIR, FT-Raman and UV-Vis spectra of ICINH were recorded in the solid phase. The optimized geometry was calculated by B3LYP method with 6-311++G(d,p) level of basis set. The harmonic vibrational frequencies, IR intensities and Raman scattering activities of the title compound were calculated at same level of theory. The scaled theoretical wavenumber showed very good agreement with the experimental values. The mulliken charges and thermodynamic functions of the ICINH were also performed at same level of theory. NLO and a study on the electronic properties such as excitation energies and wavelength, were performed by TD-DFT approach. HOMO–LUMO energy gap was also calculated and interpreted.

Keywords: ICINH, DFT, NLO, NBO, MEP

***Corresponding author**
N.RameshBabu, Department of Physics, MIET Engineering College, Tiruchirappalli – 620 007, Tamil Nadu, India.
nrbmiet@gmail.com

Received : Feb 14, 2017; **Accepted** Mar 25, 2017; **Published :** May 22, 2017;

Introduction

Indole is an aromatic heterocyclic organic compound with a bicyclic structure. It consist of a six-member benzene ring fused with five-member nitrogen containing pyrrole ring. It is of interest as it can be compared with tryptophane residue [1]. The derivative of indole is present in both-animal and plants. The most important compound of this group is tryptophan, an essential amino acid in the human diet, which a 3-substituted indole [2]. Another important indole derivative is the indole-3-acetic acid, a phytohormone, coordinating several growths processing of plants [3]. The biological activity of the indole derivatives is in connection with the nature of substitution in position 3, on the pyrrole ring [4]. Indole derivatives have an important role through individual biological functions. It is present in the side chain of amino acid tryptophan. The chemical and spectroscopic properties of indole derivatives have been subject of many experimental and theoretical investigations [5-7]. The indole tryptamine if one of the biogenic monoamines would play anti-tumor effects by either inhibiting cancer cell proliferation or stimulating the anti-cancer immunity [8]. DFT method has become an efficient tool in the prediction of molecular structure of organic molecules and in evaluating various molecular properties like conjugation, hydrogen bonding, vibrational frequencies and IR & Raman activities of the bioactive molecule [9-13].

The new Donor-π-Acceptor type dyes D_{1-3} carrying 3-(1-hexyl-1H-indol-3-yl)-2-(thiophen-2-yl) acrylonitrile as backbone with three different acceptor units were designed and synthesized by Babu, [14], using sensitizers for solar cell application. The new dyes were characterized by various spectral and elemental analyses. Their optical and electrochemical properties were investigated using spectrophotometry and cyclic voltammetry, respectively. The DFT study was carried out to investigate their Frontier MO energy states. The above study reveals that the dye carrying 4-aminobenzoic acid as an acceptor showed the highest photovoltaic efficiency among the three dyes. This can be attributed to the longer electron lifetime and lower recombination rates. Additionally, a single crystal XRD study confirms the structure of a key intermediate.

The stability of the *syn* and *anti* structures of the non-steroidal anti-inflammatory drug indomethacin were investigated by Hassan et al., [15], using the DFT/B3LYP and *ab initio* MP2 calculations with the 6-311G(d,p) basis set. The molecule indomethacin was predicted at the DFT and MP2 levels of calculation to have the *syn* ($C_1N_7C_{10}C_{18}$ ~ 40°) form being about 1.7 and 1.5 kcal/mol, respectively, lower in energy than the *anti* ($C_1N_7C_{10}C_{18}$ ~ 140°) structure. The calculated CNCC torsional angles for the chlorobenzene and indole rings *syn-anti* conformational interconversion was in a good qualitative agreement with the reported XRD angles ($C_1N_7C_{10}C_{18}$ ~ 29 and 155°) for the syn and anti conformers, respectively. Indomethacin was estimated from the calculated Gibb's free energies to have an equilibrium mixture of 95% *syn* and 5% *anti* structures at 298.15 K. The vibrational wavenumbers were calculated at the same level of theory. The complete vibrational assignments were provided on the basis of theoretical and NCA combined with experimental IR and Raman data of the molecule. The analysis of the observed spectra supported the presence of indomethacin in only one conformation at room temperature.

The (E)-2-(2-hydroxybenzylidenamino)-3-(1H-indol-3yl) propionic acid was synthesized by Saleem et al., [7]. To identify the stable structure, the theoretical conformational analysis was performed. The optimized molecular bond parameters were calculated using B3LYP/6-31G(d,p) basis set. The hyperconjugative interaction energy ($E^{(2)}$) and EDs of donor (i) and acceptor (j) bonds were calculated using NBO analysis.

The dipole moment (μ) and first order hyperpolarizability (β_0) were calculated. The band gap energy was analyzed by UV–Vis recorded spectra and compared with theoretical band gap (TD-DFT/B3LYP/6-31G(d,p)) value. The intra-molecular hydrogen bonding interaction was studied between nitrogen and hydroxyl hydrogen (N-H---O).

The molecular structure, complete vibrational spectra and the quantum mechanical calculations of the title compound were not yet reported. Therefore, the vibrational spectrum and the quantum mechanical calculations for the title compound in the ground state by DFT method with the standard 6-311++G(d,p) level of basis set were reported. Electronic absorption spectra of the title compound were predicted by using TD-DFT method. The excitation energies, wavelength and oscillator strengths were obtained at the same level of theory. Besides the molecular parameters, dipole moments, NLO, thermodynamic properties, linear polarizability and first hyperpolarizability, were calculated. The results obtained from theoretical calculations and experimental were compared.

Experimental Details

Synthesis Procedure

1H-indole-3-carbaldehyde (1.45 g, 0.01 mol) and isonicotinic acid hydrazide (1.37 g, 0.01 mol) were added to ethanol (10 ml) and stirred for an hour in the presence of hydrochloric acid to form a white precipitate. The precipitate was washed with sodium bicarbonate solution and filtered and again washed with petroleum ether (40–60%) and dried in air. The compound was recrystallized from absolute ethanol.

Results and Discussion

Molecular Geometry

The optimized structural parameters of E-[N¢-(1H-indol-3-ylmethylene) isonicotinohydrazide] are calculated using B3LYP/6-311++G(d,p) basis set and listed in Table 1. The optimized structure is shown in Fig. 1. The title molecule consists of pyridine and indole ring fused by hydrazone linkage. In ICINH, the hydrazone linkage plays an important role. For the carbonyl (C_{21}=O_{29}) bond length in hydrazone link is calculated about 1.223Å using DFT and corresponding X-ray data value is 1.236Å. The bond length of N_{18}-N_{19} is acted as bridge between the phenyl and pyridine ring and its bond length is calculated using DFT calculation at 1.368Å, while the corresponding X-rays value is 1.392Å. Similarly, the C_{21}-N_{19}/C_{16}=N_{18} bond lengths are calculated as: 1.384 : DFT; 1.330Å : X-rays data/1.288 : DFT; 1.278Å : X-rays data, respectively. In the present study, the average value of C-C bond lengths in indole ring is 1.403Å (DFT). Bikas et al., [16], observed the bond angle of O-C-C at 120.6°, which was in consistent with calculated value 121.49° (O_{29}-C_{21}-C_{22}) and its corresponding DFT value is positively deviated (~ 1°) from the calculated value. The dihedral angles are also calculated and listed in Table 1.

Vibrational Assignments

The harmonic vibrational frequencies were calculated using B3LYP/6-311++G(d,p) basis set. The title molecule belongs to C_1 point group symmetry and it had 90 vibrational normal modes of same symmetry species are listed in Table 2.1. The internal and symmetry coordinates of ICINH are listed in Table 2.1

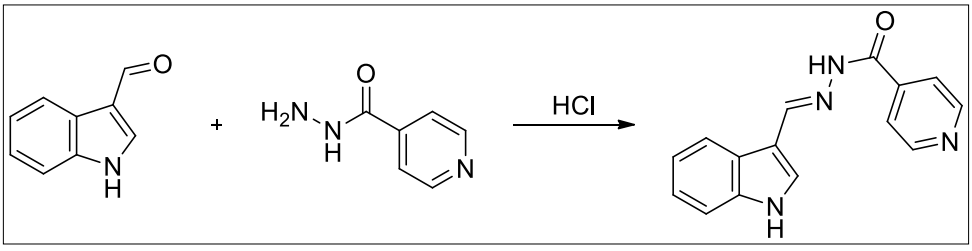

Table 1. The optimized bond parameters of ICINH using B3LYP/6-311++G(d,p)basis set

Bond Parameters	B3LYP/6-311++G(d,p)	XRD[a]
Bond Lengths (Å)		
C1-C2	1.416	
C1-C6	1.396	
C1-N15	1.383	1.347
C2-C3	1.404	
C2-C8	1.451	1.445
C3-C4	1.387	
C3-H9	1.084	
C4-C5	1.408	
C4-H10	1.084	
C5-C6	1.388	
C5-H11	1.084	
C6-H12	1.084	
C7-C8	1.385	
C7-H14	1.078	
C7-N15	1.372	
C8-C16	1.455	1.437
H13-N15	1.007	
C16-H17	1.087	
C16-N18	1.288	1.278
N18-N19	1.368	1.392
N19-H20	1.019	
N19-C21	1.384	1.33
C21-C22	1.496	1.495
C21-O29	1.223	1.236
C22-C23	1.398	
C22-C24	1.401	
C23-C25	1.388	
C23-H26	1.083	
C24-H27	1.082	
C24-N31	1.335	
C25-C28	1.394	
C25-H29	1.084	
C28-H30	1.0867	
C28-N31	1.336	
Bond Angles (°)		
C2-C1-C6	122.55	
C2-C1-N15	107.12	109.56
C6-C1-N15	130.34	
C1-C2-C3	118.87	
C1-C2-C8	107.31	

Table 1 continued from page 4

Bond Parameters	B3LYP/6-311++G(d,p)	XRD[a]
C3-C2-C8	133.81	
C2-C3-C4	118. 90	
C2-C3-H9	120.86	
C4-C3-H9	120.24	
C3-C4-C5	121.19	
C3-C4-H10	119.60	
C5-C4-H10	119.20	
C4-C5-C6	121.18	
C4-C5-H11	119.40	
C6-C5-H11	119.42	
C1-C6-C5	117.31	
C1-C6-H12	121.52	
C5-C6-H12	121.17	
C8-C7-H14	130.27	
C8-C7-N15	109.75	
H14-C7-N15	119.85	123.30
C2-C8-C7	106.01	
C2-C8-C16	123.89	130.50
C7-C8-C16	129.95	
C1-N15-C7	109.81	
C1-N15-H13	125.49	
C7-N15-H13	124.69	
C8-C16-H17	115.93	
C8-C16-N18	130.93	
H17-C16-N18	113.14	
C16-N18-N19	117.96	113.29
N18-N19-H20	119.23	
N18-N19-C21	123.39	120.33
H20-N19-C21	112.73	
N19-C21-C22	119.89	114.64
N19-C21-O29	118.60	124.70
C22-C21-O29	121.49	120.60
C21-C22-C23	117.13	
C21-C22-C24	124.87	
C23-C22-C24	117.85	
C22-C23-C25	119.05	
C22-C23-H26	119.22	
C25-C23-H26	121.73	
C22-C24-H27	120.51	
C22-C24-N31	123.46	
H27-C24-N31	116.03	
C23-C25-C28	118.39	
C23-C25-H29	121.19	
C28-C25-H29	120.41	
C25-C28-H30	120.46	

Table 1 continued from page 5

Bond Parameters	B3LYP/6-311++G(d,p)	XRD[a]
C25-C28-N31	123.50	
H30-C28-N31	116.05	
C24-N31-C28	117.73	
Dihedral Angles (°)		
C6-C1-C2-C3	-0.05	
C6-C1-C2-C8	-179.54	
N15-C1-C2-C3	179.79	
N15-C1-C2-C8	0.29	
C2-C1-C6-C5	-0.29	
C2-C1-C6-H12	179.72	
N15-C1-C6-C5	179.92	
N15-C1-C6-H12	-0.07	
C2-C1-N15-C7	-0.26	
C2-C1-N15-H13	179.33	
C6-C1-N15-C7	179.56	
C6-C1-N15-H13	-0.85	
C1-C2-C3-C4	0.41	
C1-C2-C3-H9	-179.24	
C8-C2-C3-C4	179.74	
C8-C2-C3-H9	0.09	
C1-C2-C8-C7	-0.22	
C1-C2-C8-C16	-176.16	
C3-C2-C8-C7	-179.61	
C3-C2-C8-C16	4.45	
C2-C3-C4-C5	-0.44	
C2-C3-C4-H10	179.88	
H9-C3-C4-C5	179.21	
H9-C3-C4-H10	-0.47	
C3-C4-C5-C6	0.11	
C3-C4-C5-H11	-179.77	
H10-C4-C5-C6	179.78	
H10-C4-C5-H11	-0.09	
C4-C5-C6-C1	0.26	
C4-C5-C6-H12	-179.75	
H11-C5-C6-C1	-179.87	
H11-C5-C6-H12	0.12	
H14-C7-C8-C2	-175.75	
H14-C7-C8-C16	-0.14	
N15-C7-C8-C2	0.06	
N15-C7-C8-C16	175.67	
C8-C7-N15-C1	0.12	
C8-C7-N15-H13	-179.48	
H14-C7-N15-C1	176.44	
H14-C7-N15-H13	-3.16	
C2-C8-C16-H17	20.44	

Table 1 continued from page 6

Bond Parameters	B3LYP/6-311++G(d,p)	XRD[a]
C2-C8-C16-N18	-158.81	
C8-C16-N18-N19	-154.47	
H17-C16-N18-N19	26.29	
C16-N18-N19-H20	2.17	
C16-N18-N19-C21	-177.10	
N18-N19-C21-C22	21.38	
N18-N19-C21-O32	175.42	
H20-N19-C21-C22	21.29	
H20-N19-C21-O32	-160.76	
N19-N21-C22-C23	176.81	
N19-N21-C22-C24	-5.23	
O32-C21-C22-C23	-156.35	
O32-C21-C22-C24	28.10	
C21-C22-C23-C25	25.76	
C21-C22-C23-H26	-149.79	
C24-C22-C23-C25	-177.41	
C24-C22-C23-H26	2.29	
C21-C22-C24-H27	-1.54	
C21-C22-C24-N31	178.16	
C23-C22-C24-H27	-3.35	
C23-C22-C24-N31	175.99	
C22-C23-C25-C28	-178.87	
C22-C23-C25-H29	0.47	
H26-C23-C25-C28	1.25	
H26-C23-C25-H29	-179.20	
C22-C24-N31-C28	-178.45	
H27-C24-N31-C28	1.10	
C23-C25-C28-H30	0.92	
C23-C25-C28-N31	-179.72	
H29-C25-C28-H30	179.80	
H29-C25-C28-N31	0.18	
C25-C28-N31-C24	0.25	
H30-C28-N31-C24	-179.37	

[a] Zuo-Liang Jing, Wen-Wen, Cheng, Xin Chen and Yu Ming, 200-(1H-Indol-3-ylmethylene)isonicotinohydrazide ethanol solvate, Acta Cryst. (2006). E62, o1360–o1361.

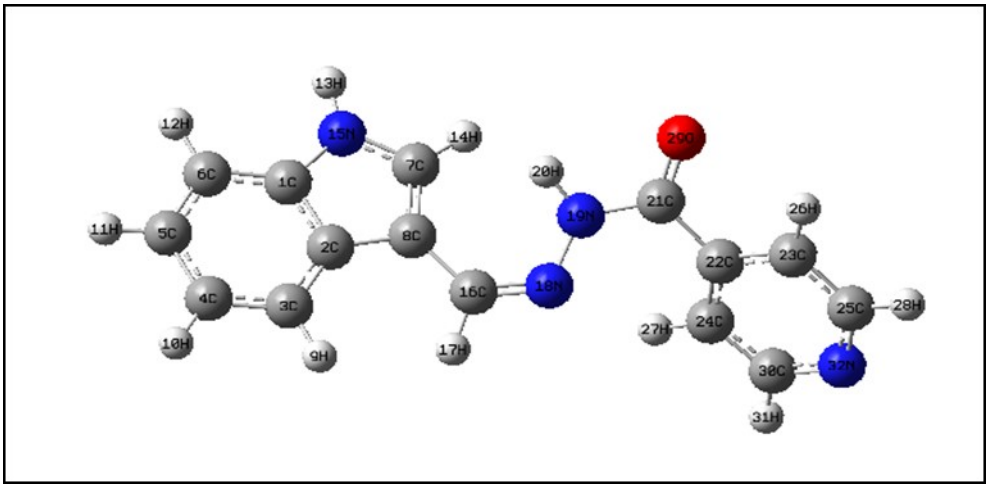

Fig. 1. The optimized molecular structure of ICINH

and 2.2, respectively. The percentage of PED obtained from MOLVIB program package was used for assigning vibrational peaks. The exclusion of anharmonicity factor and the level of basis set used, certain theoretical frequencies are not matched with that of the experimental values. Hence linear scaling procedure is adopted to scale down the frequency values. In this study, we have followed scaling factor of 0.968 for DFT [17]. The observed FT-IR, FT-Raman and simulated spectra of ICINH are shown in Figs. 2 and 3, respectively.

Ring Vibrations

The ring stretching vibrations are very prominent in the spectrum of pyridine and its derivatives and are highly characteristics of aromatic ring itself [18]. The C–C stretching vibrations of pyridine derivatives usually appear in the region between 1650–1400 cm^{-1} and 1100–1000 cm^{-1} [19]. In the present study, the peaks identified at 1006 cm^{-1} in FT-IR and 1009 cm^{-1} in FT-Raman are assigned to C–C stretching vibrations. Due to the absence of peaks, the theoretically scaled values at 1553, 1318 and 1025 cm^{-1} are assigned as C–C stretching vibrations of the rest of other modes in pyridine ring .The presence of nitrogen in the ring of the pyridine structure gives rise to two C–N stretching vibrations. Identifying these vibrations is rather a difficult task as their vibrational frequency lies within the C–C stretching region. As expected, the peaks for C–N stretching vibrations are found at 1244 cm^{-1} in FT-IR and 1254 cm^{-1} in FT-Raman spectrum. The theoretically scaled values of this mode are found to be in good agreement with experimental values.

According to PED results, the C–C stretching vibrations of six and five members are assigned. The C–C stretching vibrations are observed at 1608, 1501 and 1336 cm^{-1} in FT-IR and 1606, 1563, 1345 and 1284 cm^{-1} in FT-Raman spectrum. The theoretically predicted scaled values are in excellent correlation with that of the experimental values.

C–H Vibrations

Four C–H bonds in the pyridine ring of the title molecule give rise to four C–H stretching vibrations. The hetero-aromatic structure shows the presence of C–H stretching vibrations in the region 3000–3100 cm^{-1} [20], which is the characteristic region for ready identification of this structure. In this region, the bands are not affected appreciably by the nature of the substituents. In the present study, the peak at 3107 cm^{-1} in FT-IR and at 3109 cm^{-1} in FT-Raman are assigned to C–H stretching vibrations of the pyridine ring. The percentage of PED results show that these modes are

Table 2.1. Possible internal co-ordinates of ICINH

S.No	Type	Fragment type	Definition
1-8	C-C	Double ring	C_1-C_2, C_2-C_3, C_3-C_4, C_4-C_5, C_5-C_6, C_6-C_1, C_2-C_8, C_7-C_8
9,10	C-N		C_1-N_{15}, C_7-N_{15}
11-15	C-H		C_3-H_9, C_4-H_{10}, C_5-H_{11}, C_6-H_{12}, C_7-H_{14}
16	N-H		N_{15}-H_{13}
17-20	C-C	Pyridine ring	C_{22}-C_{23}, C_{22}-C_{24}, C_{23}-C_{25}, C_{25}-C_{28}
21,22	C-N		C_{24}-N_{31}, C_{28}-N_{31}
23-26	C-H		C_{23}-H_{26}, C_{24}-H_{27}, C_{25}-H_{29}, C_{28}-H_{30}
27,28	C-C	Out-of the ring	C_8-C_{16}, C_{21}-C_{22}
29	C=O		C_{21}-O_{32}
30	N-H		N_{19}-H_{20}
31	C-H		C_{16}-H_{17}
32,33	C-N		C_{16}-N_{18}, C_{21}-N_{19}
34	N-N		N_{18}-N_{19}
In-plane bending			
35-45	C-C(N)-C(N)	Double ring	C_1-C_2 -C_3, C_2-C_3-C_4, C_3-C_4 -C_5, C_4-C_5 -C_6, C_5-C_6 -C_1, C_6-C_1-C_2, C_1-C_2-C_8, C_2-C_8-C_7, C_8-C_7-N_{15}, C_7-N_{15}-C_1 N_{15}-C_1 -C_2
46-55	C(N)-C-H		C_2-C_3 -H_9, C_4-C_3 -H_9, C_3-C_4 -H_{10}, C_5-C_4 -H_{10}, C_4-C_5 -H_{11}, C_6-C_5 -H_{11}, C_1-C_6 -H_{12}, C_5-C_6 -H_{12}, C_8-C_7 -H_{14}, N_{15}-C_7 -H_{14}
56,57	C-N-H		C_1-N_{15}-H_{13}, C_7-N_{15}-H_{13}
58,59	C-C-C(N)		C_6-C_1-N_{15}, C_3-C_2-C_8
60,61	C-C-H	Out-of the ring	C_8-C_{16}-H_{17}, N_{18}-C_{16}-H_{17}
62,63	C-C-N		C_8-C_{16}-N_{18}, C_{22}-C_{21}-N_{19}
64,65	C-N-N		C_{16}-N_{18}-N_{19}, C_{21}-N_{19}-N_{18}
66,67	C(N)-N-H		C_{21}-N_{19}-H_{20}, N_{18}-N_{19}-H_{20}
68,69	C(N)-C=O		C_{22}-C_{21}-O_{32}, N_{19}-C_{21}-O_{32}

Table 2.1 continued from page 9

S.No	Type	Fragment type	Definition
70-73	C-C-C		C_{21}-C_{22} -C_{23}, C_{21}-C_{22}-C_{24}, C_2-C_8 -C_{16}, C_7-C_8-C_{16}
74-79	C-C(N)-C(N)	Pyridine ring	C_{22}-C_{23} -C_{25}, C_{23}-C_{25}-C_{28}, C_{25}-C_{28} -N_{31}, C_{28}-N_{31}-C_{24}, N_{31}-C_{24}-C_{22}, C_{24}-C_{22}-C_{23}
80-87	C(N)-C-H		C_{22}-C_{23}-H_{26}, C_{25}-C_{23}-H_{26}, C_{22}-C_{24}-H_{27}, N_{31}-C_{24} -H_{27}, C_{23}-C_{25}-H_{29}, C_{28}-C_{25}-H_{29}, C_{25}-C_{28}-H_{30}, N_{31}-C_{28}-H_{30}
Out-of-plane bending			
88-98	C(N)-C(N)-C(N)-C(N)	Double ring	C_1-C_2-C_3-C_4, C_2-C_3-C_4-C_5, C_3-C_4-C_5-C_6, C_4-C_5 -C_6-C_1, C_5-C_6-C_1-C_2, C_6-C_1-C_2-C_3, C_1-C_2 -C_8-C_7, C_2-C_8-C_7-N_{15}, C_8-C_7-N_{15}-C_1, C_7-N_{15}-C_1-C_2, N_{15}-C_1 -C_2-C_8
99-103	H-C(N)-C-C(N)		H_9-C_3-C_2-C_4, H_{10}-C_4-C_3-C_5, H_{11}-C_5-C_4-C_6, H_{12}-C_6-C_1-C_5, H_{13}-N_{15}-C_1-C_7, H_{14}-C_7-C_8-N_{15}
105,106	C-C-C-C	Out-of the ring	C_{16}-C_8-C_2-C_7, C_{21}-C_{22}-C_{23}-C_{24}
107	O-C-C-N		O_{32}-C_{21}-C_{22}-N_{19}
108	H-N-N-C		H_{20}-N_{19}-N_{18}-C_{21}
109	H-C-C-N		H_{17}-C_{16}-C_8-N_{18}
110	C-N-N-C		C_{16}-N_{18}-N_{19}-C_{21}
111-114	N-C-C-C		N_{19}-C_{21}-C_{22}-C_{23}, N_{19}-C_{21}-C_{22}-C_{24}, C_2- C_8- C_{16}-N_{18}, C_7-C_8-C_{16}-N_{18}
115-120	C(N)-C(N)-C(N)-C(N)	Pyridine	C_{22}-C_{23}-C_{25}-C_{28}, C_{23}-C_{25}-C_{28}-N_{31}, C_{25}-C_{28}-N_{31}-C_{24}, C_{28}-N_{31}-C_{24}-C_{22}, N_{31}-C_{24}-C_{22}-C_{23}, C_{24}-C_{22}-C_{23}-C_{25}
121-124	H-C-C-C		H_{26}-C_{23}-C_{22}-C_{25}, H_{27}-C_{24}-C_{22}-N_{31}, H_{29}-C_{25}-C_{23}-C_{28}, H_{30}-C_{28}-C_{25}-N_{31}
125,126	C(N)-C-C-C	Torsion	C_3-C_2-C_8-C_{16}, N_{15}-C_7-C_8-C_{16}
127,128	C-C-C-C(N)	Butterfly	C_8-C_2-C_1-C_6, C_3-C_2-C_1-N_{15}

Table. 2.2. Local Symmetry coordinates of ICINH

S.No	Type	Fragment type	Definition
1-8	C-C	Double ring	R_1, R_2, R_3, R_4, R_5, R_6, R_7, R_8
9,10	C-N		R_9, R_{10}
11-15	C-H		R_{11}, R_{12}, R_{13}, R_{14}, R_{15}
16	N-H		R_{16}
17-20	C-C	Pyridine ring	R_{17}, R_{18}, R_{19}, R_{20}
21,22	C-N		R_{21}, R_{22}
23-26	C-H		R_{23}, R_{24}, R_{25}, R_{26}
27,28	C-C	Out-of the ring	R_{27}, R_{28}
29	C=O		R_{29}
30	N-H		R_{30}
31	C-H		R_{31}
32,33	C-N		R_{32}, R_{33}
34	N-N		R_{34}
In-plane bending			
35	C(N)-C(N)-C(N)	Double ring	$(\beta_{35} - \beta_{36} + \beta_{37} - \beta_{38} + \beta_{39} - \beta_{40})/\sqrt{6}$
36			$(-\beta_{35} - \beta_{36} + 2\beta_{37} - \beta_{38} + \beta_{39} - 2\beta_{40})/\sqrt{12}$
37			$(\beta_{35} - \beta_{36} - \beta_{38} - \beta_{39})/\sqrt{2}$
38			$\beta_{41} + a(\beta_{42} + \beta_{45}) + b(\beta_{43} + \beta_{44})$
39			$(a - b)(\beta_{41} - \beta_{44}) + (1 - a)(\beta_{42} - \beta_{43})$

Table 2.2 continued from page 11

S.No	Type	Fragment type	Definition
40-44	C(N)-C-H		$(\beta_{46}-\beta_{47})/\sqrt{2}$, $(\beta_{48}-\beta_{49})/\sqrt{2}$, $(\beta_{50}-\beta_{51})/\sqrt{2}$, $(\beta_{52}-\beta_{53})/\sqrt{2}$,
45	C-N-H		$(\beta_{56}-\beta_{57})/\sqrt{2}$
46,47	C(N)-C(N)-C(N)		b_{58}, b_{59}
48	C-C-H	Out-of the ring	$(\beta_{60}-\beta_{61})/\sqrt{2}$
49,50	C-C-N		b_{62}, b_{63}
51	C-N-N		$(\beta_{64}-\beta_{65})/\sqrt{2}$
52	C(N)-N-H		$(\beta_{66}-\beta_{67})/\sqrt{2}$
53	C(N)-C=O		$(\beta_{68}-\beta_{69})/\sqrt{2}$
54,55	C-C-C		$(\beta_{70}-\beta_{71})/\sqrt{2}$, $(\beta_{72}-\beta_{73})/\sqrt{2}$
56	C-C(N)-C(N)	Pyridine ring	$(\beta_{74}-\beta_{75}+\beta_{76}-\beta_{77}+\beta_{78}-\beta_{79})/\sqrt{6}$
57			$(-\beta_{74}-\beta_{75}+2\beta_{76}-\beta_{77}-\beta_{78}+2\beta_{79})/\sqrt{12}$
58			$(\beta_{74}-\beta_{75}-\beta_{77}-\beta_{78})/2$
59-62	C(N)-C-H		$(\beta_{80}-\beta_{81})/\sqrt{2}$, $(\beta_{82}-\beta_{83})/\sqrt{2}$,
Out-of-plane bending			
63	C(N)-C(N)-C(N)-C(N)	Double ring	$(\gamma_{88}-\gamma_{89}+\gamma_{90}-\gamma_{91}+\gamma_{92}-\gamma_{93})/\sqrt{6}$
64			$(-\gamma_{88}+2\gamma_{89}-\gamma_{90}-\gamma_{91}+2\gamma_{92}-\gamma_{93})/\sqrt{12}$
65			$(\gamma_{88}-\gamma_{89}+\gamma_{90}-\gamma_{91})/\sqrt{2}$
66			$b(\gamma_{94}+\gamma_{98})+a(\gamma_{95}+\gamma_{97})+\gamma_{96}$

Table 2.2 continued from page 12

S.No	Type	Fragment type	Definition
67			$(a-b)(\gamma_{98}-\gamma_{94})+(1-a)(\gamma_{97}-\gamma_{95})$
68-73	H-C(N)-C-C(N)		g_{99}, g_{100}, g_{101}, g_{102}, g_{103}, g_{104}
74,75	C-C-C-C	Out-of the ring	g_{105}, g_{106}
76	O-C-C-N		g_{107}
77	H-N-N-C		g_{108}
78	H-C-C-N		g_{109}
79	C-N-N-C		g_{110}
80,81	N-C-C-C		$(\gamma_{111}-\gamma_{112})/\sqrt{2}$, $(\gamma_{113}-\gamma_{114})/\sqrt{2}$
82	C(N)-C(N)-C(N)-C(N)	Pyridine	$(\gamma_{115}-\gamma_{116}+\gamma_{117}-\gamma_{118}+\gamma_{119}-\gamma_{120})/\sqrt{6}$
83			$(\gamma_{115}-\gamma_{117}+\gamma_{118}-\gamma_{119})/2$
84			$(-\gamma_{115}+2\gamma_{116}-\gamma_{117}-\gamma_{118}+2\gamma_{119}-\gamma_{120})/\sqrt{12}$
85-88	H-C-C-C		g_{121}, g_{122}, g_{123}, g_{124}
89	C(N)-C-C-C	Ring Torsion	$(\gamma_{125}-\gamma_{126})/\sqrt{2}$
90	C-C-C-C(N)	Butterfly	$(\gamma_{127}-\gamma_{128})/\sqrt{2}$

Table 2.3. The experimental and calculated frequencies of ICINH using B3LYP/6-311++G(d,p) level of basis set [harmonic frequencies (cm^{-1}), IR, Raman intensities (Km/mol), reduced masses (amu) and force constants ($mdynA°^{-1}$)]

Mode No	Exp. IR	Exp. Raman	Frequencies	Scaled frequencies	Red. Masses	Force constants	IR Intensity	Raman Intensity	Vibrational Assignments
1	-	-	23	22	5.6685	0.0017	0.05	41.46	gring (90)
2	-	-	31	30	6.2039	0.0035	0.26	47.75	gring (93)
3	-	-	38	37	4.7887	0.0041	0.29	50.62	$g_{(py)}$ring (97)
4	-	-	73	70	6.1906	0.0192	0.52	0.88	$g_{(py)}$ring (98)
5	-	89	93	90	6.2748	0.0318	0.06	10.04	gring (89)
6	-	-	132	128	6.7417	0.0692	0.31	3.54	gC=O (69), gring (23)
7	-	-	151	146	5.367	0.0716	0.35	3.71	gring (66), gN–N (26)
8	-	-	171	166	4.8316	0.0835	0.20	5.00	gN–N(54), gring (37)
9	-	-	196	190	5.1729	0.1176	0.19	3.45	$g_{(py)}$ring (67), Butterfly (21)
10	-	-	223	216	4.1358	0.1213	2.07	1.51	Butterfly (89)
11	-	-	236	229	5.5815	0.1835	2.48	4.94	$\beta_{(py)}$ring (78)
12	-	-	295	285	7.0353	0.3595	0.36	0.27	tring (94)
13		-	376	363	5.8348	0.4847	0.80	0.48	gring (62), g_{out}C–C(21)
14	-	-	402	389	3.5462	0.3379	0.58	1.55	g_{out}C–N(43), gN–N(18), gring(14)
15	-	-	418	405	5.2085	0.5367	0.63	1.35	gring (69), $g_{(py)}$ring (24)
16	-	-	426	412	2.5799	0.2753	6.89	0.44	g_{out}C–C(50), bC–N(22), bN–H(10)
17	426	-	440	426	1.5194	0.1731	7.82	0.87	gN–H(78)
18	-	-	449	434	3.4966	0.415	3.38	0.38	g_{out}C–C(56), gC–H (22)

Table 2.3 continued from page 14

Mode No	Exp. IR	Exp. Raman	Frequencies	Scaled frequencies	Red. Masses	Force constants	IR Intensity	Raman Intensity	Vibrational Assignments
19	-	-	498	482	5.8526	0.8561	0.62	1.60	βring (49),g_{out}C–C(19), gring (18)
20	-	-	552	535	5.1322	0.9221	1.85	2.76	gC=N(61), gring (26)
21	-	-	563	545	5.496	1.0281	0.54	2.03	βring (72)
22	-	-	582	564	2.8828	0.5762	1.76	4.01	β_{out}C-C (46), βN–H (23)
23	-	-	589	570	3.2755	0.6698	7.32	2.24	g_{out}N–H(63), βC–H (18)
24	581	-	606	587	5.2868	1.1458	11.97	3.94	$\beta_{(py)}$ring (68), g_{out}N–H(22)
25	615	-	637	616	6.325	1.5108	2.52	1.88	β_{out}C-C (58), βC–H (20), βN–H (14)
26	-	-	643	623	2.7471	0.6694	0.95	1.01	βring (52), gC–H (24)
27	-	-	668	647	2.6474	0.6964	2.08	15.49	βN-N (50), βC–N (18), $\beta_{(py)}$ring (14)
28	682	-	702	679	4.4972	1.3055	1.36	2.28	βring (51), $\beta_{(py)}$ring (27)
29	-	-	719	696	2.1818	0.6637	3.21	0.31	β_{out}C-C (47), β_{out}C–H (20), βring (17)
30	-	-	748	724	3.0533	1.0053	12.23	4.31	β_{out}C-N (57), β_{py}ring (18), βC=O (13)
31	-	-	751	727	1.4353	0.477	18.39	0.67	gC-H (79)
32	-	-	754	730	4.3578	1.4603	3.85	4.77	gC-H (74), $\beta_{(py)}$ring (13)
33	752	-	774	749	3.9285	1.3867	0.53	1.49	β_{out}C-H (48), βring (21)
34	-	-	784	759	4.6888	1.6972	4.98	9.52	βring (56), $\beta_{(py)}$ring (23)
35	793	795	828	802	1.3744	0.5555	1.89	1.51	gC-H (88)
36	-	-	840	813	1.9452	0.808	2.26	1.91	$g_{(py)}$C-H (92)
37	830	-	855	828	1.4952	0.6446	0.98	0.25	βC=O (60), $\beta_{(py)}$ring (19)
38	-	-	877	849	3.9613	1.796	23.55	3.59	βC=N (45), βring (24), $\beta_{(py)}$ring (18)
39	-	-	893	864	4.4426	2.0861	3.75	0.23	βring (78)
40	-	-	919	890	1.4668	0.7301	1.25	6.07	gC-H (91)
41	912	-	944	913	1.3666	0.717	0.23	0.11	gC-H (87)
42	-	-	949	919	1.3956	0.7404	0.86	0.11	$g_{(py)}$C-H (90)
43	-	-	981	949	1.2808	0.7258	0.01	0.06	bN-H (59), bC–H(21)
44	953	-	986	955	1.4487	0.8303	0.17	0.01	$g_{(py)}$C-H (92)
45	-	-	1006	974	1.3774	0.8218	0.47	0.09	$g_{(py)}$C-H (92)
46	-	-	1035	1002	2.1293	1.3435	1.87	6.90	uC-C (41), βC–H (28)
47	1006	1009	1040	1007	4.2574	2.715	2.20	2.57	$u_{(py)}$C-C (52), $\beta_{(py)}$C–H (29)
48	-	-	1059	1025	3.2592	2.1539	0.09	13.50	$u_{(py)}$C-C (68), $\beta_{(py)}$C–H (24)

OPEN ACCESS
Freely Available Online

OpenAccessPub

Table 2.3 continued from page 15

Mode No	Exp. IR	Exp. Raman	Frequencies	Scaled frequencies	Red. Masses	Force constants	IR Intensity	Raman Intensity	Vibrational Assignments
49	1047	1041	1066	1032	4.5472	3.0425	4.45	1.84	υ_{out}C-C (45), βring (20), βC–H (14)
50	-	-	1109	1074	3.4326	2.4881	18.31	16.64	υN-N(52), $\beta_{(py)}$C–H (18), β_{out}C–H (13)
51	-	1092	1129	1093	1.5981	1.2012	5.03	1.73	β C-H (47), βN–H (22), υC–N(17)
52	-	-	1139	1102	1.4616	1.1167	0.86	0.43	$\beta_{(py)}$C-H (50), $\upsilon_{(py)}$C–C (27)
53	-	-	1155	1118	1.4763	1.1596	8.68	0.69	βC-H (69)
54	1126	1125	1160	1123	2.4869	1.9719	14.10	1.24	υ_{out}C-C (42), υ_{out}C–N (28) $\beta_{(py)}$C–H (15),
55	-	-	1178	1140	1.1543	0.9431	0.36	0.39	υC-C (53), υC–N (19), βC–H (15)
56	-	-	1225	1186	1.4787	1.3081	2.73	1.51	$\beta_{(py)}$C-H (72), $\upsilon_{(py)}$C–N (20)
57	-	-	1251	1211	2.7583	2.5422	12.80	0.79	βC-H (52), υC–N(18), βN–H (14)
58	-	-	1263	1222	1.8362	1.7252	7.35	10.89	υC-N (54), βC–H (31)
59	1244	1254	1285	1244	7.2124	7.0219	2.07	1.25	$\upsilon_{(py)}$C-N (59), $\beta_{(py)}$C–H (22)
60	-	1284	1325	1282	2.4286	2.5111	0.37	5.82	υC-C (62), βC–H (20)
61	1298	-	1339	1296	2.3836	2.5178	54.46	0.89	β C–H (49), υC–N(19), β_{out}C–H (17)
62	-	-	1361	1318	3.0228	3.3	71.69	18.10	$\upsilon_{(py)}$ C–C (50), βC–H (21), υ_{out}C–C (12)
63	-	-	1365	1322	1.2876	1.4144	0.50	0.80	υ_{out}C–N (58), βC–H (23)
64	1336	1345	1371	1327	5.9533	6.5908	6.32	4.61	υC–C (72), βC–H (21)
65	1360	1368	1410	1364	1.5509	1.8154	16.15	8.86	b_{out}C–H (59), υC–N (15), βN–H (12)
66	-	-	1442	1396	2.1721	2.6626	6.54	4.66	υC–C (49), βC–H (27)
67	1408	-	1447	1401	2.2447	2.7699	2.37	1.22	$\beta_{(py)}$C–H (65), $\upsilon_{(py)}$ (24)
68	-	-	1473	1426	1.7655	2.2568	30.11	9.65	β_{out}N-H (60), υ_{out}C-N (17), υ_{out}C–C (14)
69	-	-	1483	1436	2.3645	3.064	4.89	0.81	βC-H (54), υC-C (21), β_{out}N–H (18)
70	1447	1455	1508	1460	2.2353	2.9957	1.61	3.14	$\beta_{(py)}$ C-H (48), $\upsilon_{(py)}$ (23), υ_{out}C-C (10)
71	-	-	1524	1475	2.7967	3.8252	0.94	0.21	υC–N (43), υC–C (24), βC–H (18)
72	1501	-	1554	1505	4.4312	6.307	20.77	41.94	υC=C (68), βC–H (19)
73	-	-	1604	1553	5.2119	7.9032	1.13	0.34	$\upsilon_{(py)}$ C–C (69), βC–H (22)
74	-	1563	1615	1563	5.7905	8.8973	0.09	6.24	υC–C (53), βN–H (25)
75	-	-	1628	1575	5.6711	8.851	11.33	13.99	$\upsilon_{(py)}$ C–N (56),$\upsilon_{(py)}$C–C (23),$\beta_{(py)}$C–H(14)
76	-	-	1657	1604	7.6432	12.3614	5.91	100.00	$\upsilon_{out.}$C=N (56), υC–C (23), βC–H (14)

www.openaccesspub.org | JNDC CC-license DOI : 10.14302/issn.2377-2549.jndc-17-1459 Vol-1 Issue –3 Page No– 16

Table 2.3 continued from page 16

Mode No	Exp. IR	Exp. Raman	Frequencies	Scaled frequencies	Red. Masses	Force constants	IR Intensity	Raman Intensity	Vibrational Assignments
77	1608	1606	1658	1605	6.6961	10.8407	2.95	28.60	υC−C (52), υC=N (28), βC−H (12)
78	1677	-	1718	1663	7.9762	13.8766	100.00	14.72	υC=O (71), βN−H (23)
79	-	-	3147	3046	1.0879	6.3482	1.02	0.82	$\upsilon_{out.}$C−H (98)
80	-	-	3150	3049	1.0892	6.366	4.06	2.60	$\upsilon_{as(py)}$ C−H (95)
81	-	-	3167	3066	1.0858	6.4172	0.15	0.55	υ_{as}C−H (96)
82	3078	-	3174	3073	1.0887	6.463	0.72	2.26	υ_{as}C−H (96)
83	-	-	3184	3082	1.0936	6.532	4.39	1.24	υ_{as}C−H (95)
84	-	-	3185	3083	1.0909	6.5186	2.94	2.80	$\upsilon_{as(py)}$C−H (92)
85	-	-	3194	3092	1.0971	6.5933	3.03	5.67	υ_{s}C−H (97)
86	-	-	3201	3099	1.092	6.593	2.66	0.24	$\upsilon_{as(py)}$C−H (91)
87	3107	3109	3202	3100	1.0948	6.6134	0.13	3.81	$\upsilon_{as(py)}$C−H (94)
88	3159	-	3253	3149	1.097	6.8395	0.27	0.60	υC−H (99)
89	-	-	3471	3360	1.0748	7.6289	7.50	3.16	$\upsilon_{out.}$N−H (99)
90	3531	-	3664	3540	1.0805	8.5473	21.55	1.77	υN−H (100)

n: Stretching, β: in-plane-bending, Γ: out-of-plane bending, τ: Torsion, vw: very week, w: week, m: medium, s: strong, vs: very strong,
[a] Scaling factor: 0.9608 (Radom et al., 1970 and Pople et al., 1993),
[b] Relative IR absorption intensities normalized with highest peak absorption equal to 100,
[c] Relative Raman intensities calculated by Equation (2.1) and normalized to 100,
[d] Total energy distribution calculated at B3LYP/6-311++G(d,p) level.

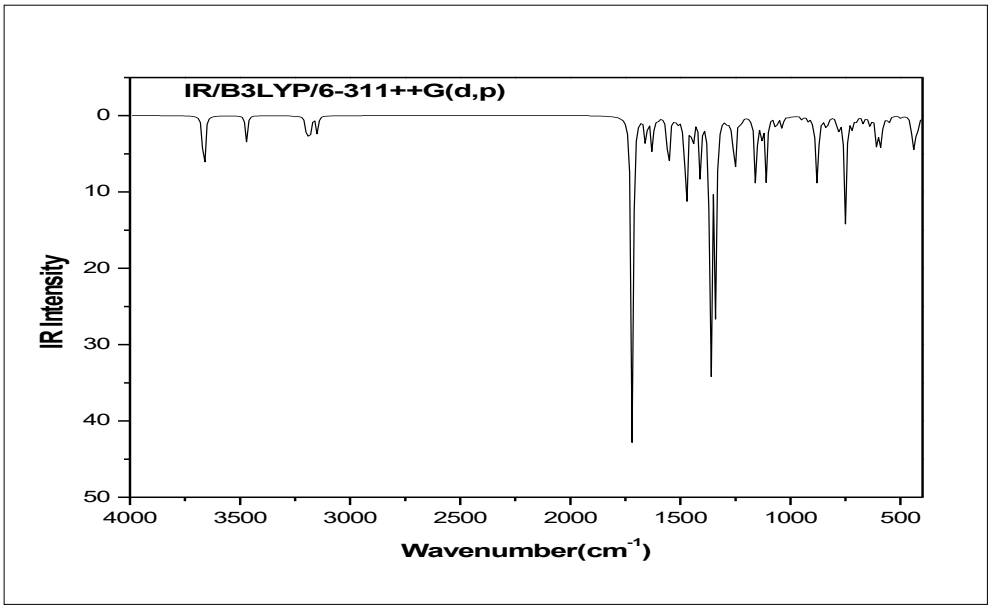

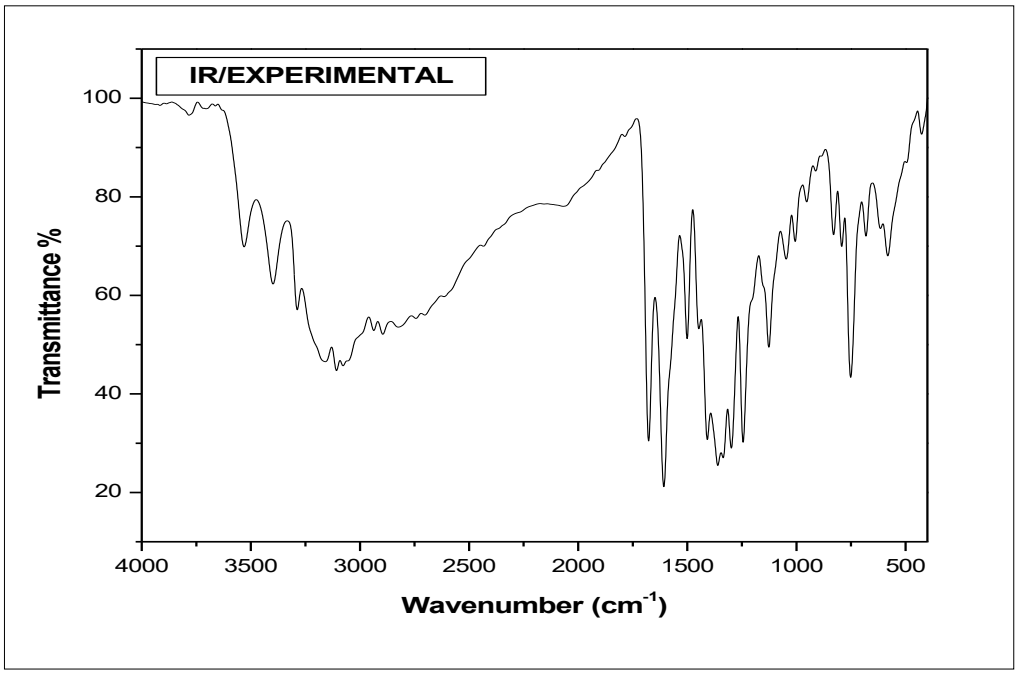

Fig. 2. The combined theoretical and experimental FT-IR spectra of ICINH

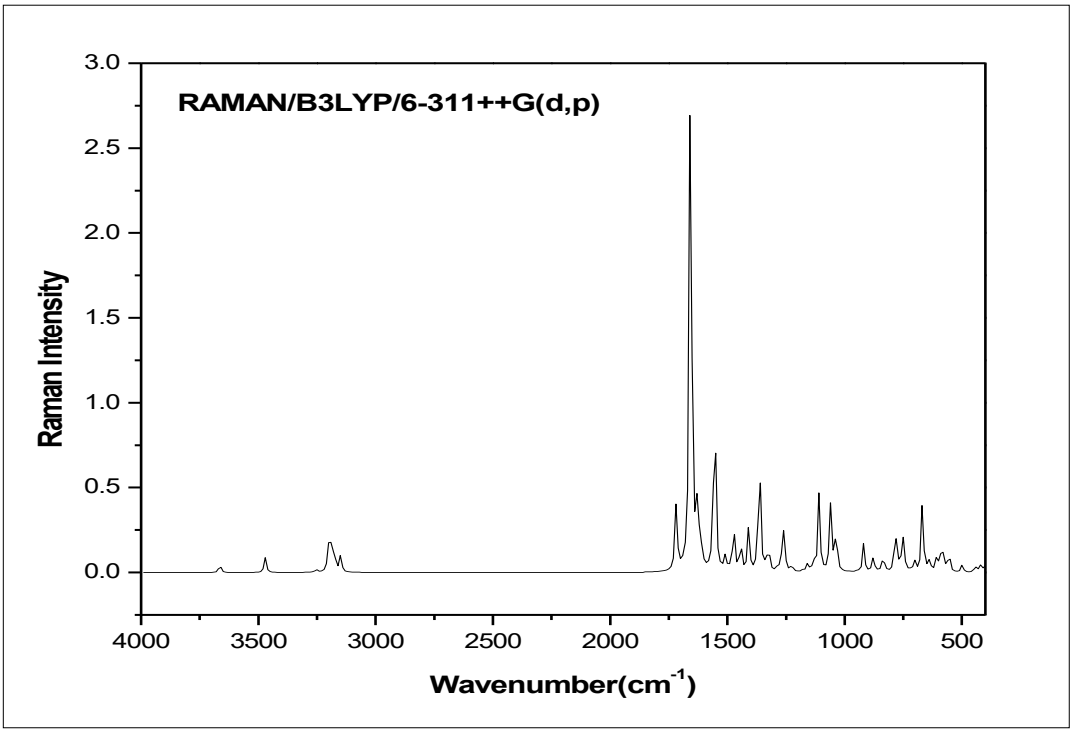

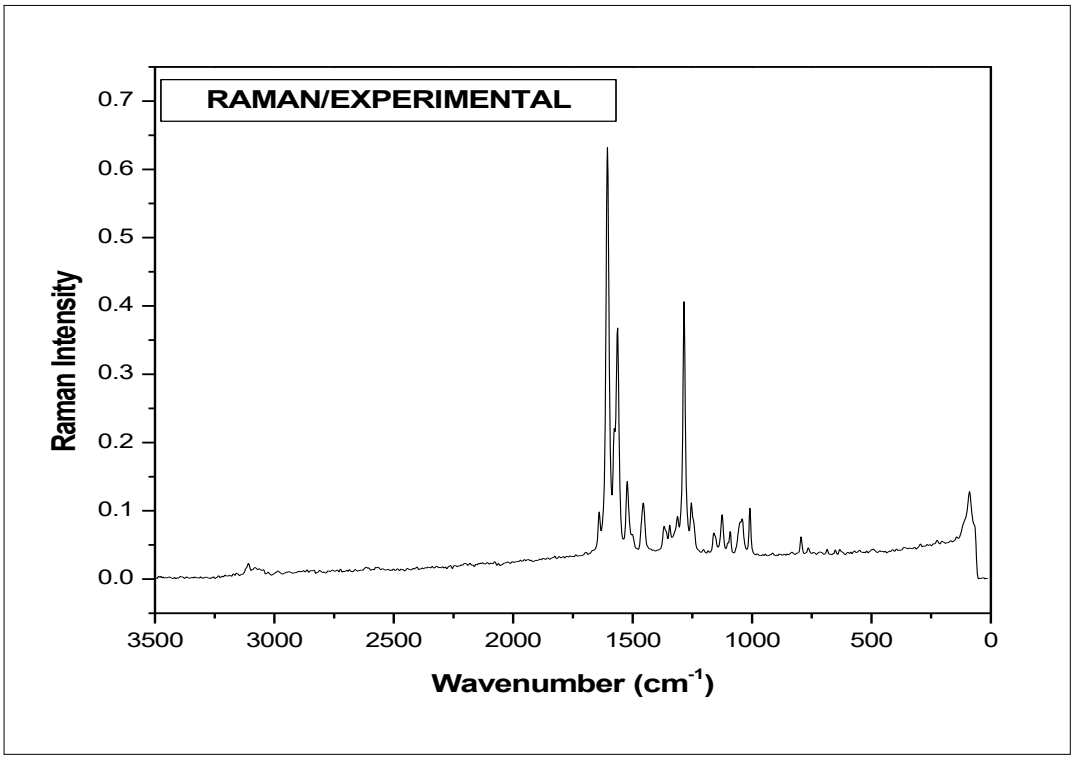

Fig. 3. The combined theoretical and experimental FT-Raman spectra of ICINH

very pure modes. Similarly, the peaks appeared at 3159 and 3078 cm^{-1} in FT-IR are ascribed to C–H stretching vibrations of the benzene ring of the title molecule.

C=O Vibrations

The characteristic IR absorption wavenumber of C=O is normally strong in intensity and found in the region 1600–1800 cm^{-1} [21,22]. In the present study, the strong peak at 1677 cm^{-1} in FT-IR is assigned to C=O stretching. The calculated value of C=O stretching mode at B3LYP/6-311++G(d,p) shows good agreement with the experimental value. The C=O in-plane bending vibration is identified at 830 cm^{-1} in FT-IR. A peak for C=O out-of-plane bending vibration is not active in both IR and Raman spectra. Hence the theoretically predicted value (128 cm^{-1}/mode no: 6) is assigned to this mode.

N–H Vibrations

In primary amines, usually the N–H stretching vibrations occur in the region 3600–3300 cm^{-1} [23]. In the present study, the N–H bond in the five member ring produce a well defined peak at 3531 cm^{-1} in FT-IR. A peak for the N_{19}–H_{20} bond present at the out-of-the ring is not active in both IR and Raman. Hence, the theoretical scaled value of 3540 cm^{-1} is assigned to N_{15}–H_{13} stretching mode. All the vibrations in this group are in excellent agreement with experimental results as well as with literature [24].

C=N and N–N Vibrations

The identification of C=N stretching vibrations are difficult task since these are usually coupled with ring stretching and C-H in-plane bending vibrations. A bond C_{21}=N_{19} at out of the ring possesses three vibrational normal modes. Since all these vibrations are inactive in both the spectra, the theoretically predicted wavenumbers 1604, 849 and 535 cm^{-1} are ascribed to C=N stretching, in-plane bending and out-of-plane bending, respectively. Similarly, the N–N stretching and bending vibrations are not present in both IR and Raman. Hence, the theoretically scaled values of 1074, 647 and 166 cm^{-1} are attributed to N–N stretching, in-plane bending and out-of-plane bending vibrations, respectively.

NLO Property

Non linear effect arise from the interactions of electromagnetic fields in various media to produce new fields altered in phase, frequency, amplitude or other propagation characteristics from incident fields [25]. The first hyperpolarizability (β_0), dipole moment μ and polarizability α are calculated using DFT/6-311++G(d,p) basis set. The computed total static dipole moment (μ), the mean polarizability (α_0) the mean first hyperpolarizability (β_0), for the molecule under study are presented in Table 3 shows that the first order hyperpolarizability value play an important role in determining the NLO activity of the molecule. The first order hyper polarizability (β_0) of the present molecule is $8.6424x10^{-30}$ esu while that of urea is $0.3728x10^{-30}$ esu. The (β_0) of ICINH is 23 times greater than that of urea, hence, the molecule can be said to be highly NLO activity; which is naturally due to the contribution of oxygen atom which makes one part of molecule highly negative and other part as equally positive.

NBO Analysis

The NBO analysis is performed on ICINH using B3LYP/6-311++G(d,p) basis set and are listed in Table 4. In the study, the π bonds have higher ED than the σ bonds. Due to this reason, the σ-σ* transitions have minimum delocalization energy than the π-π* transitions. It is evident from the Table 4. The ED of π (C_{30}-N_{32}) bond transfer energy 116.4, 52.38 kJ/mol to the acceptor orbitals: C_{22}-C_{24} and C_{23}-C_{25}, respectively. There occurs a strong intra-molecular hyperconjugative interaction of π electron from C_{23}-C_{25} bond to the π*C_{22}-C_{24}→C_{30}-N_{32} bonds, which increases the EDs: 0.3281 and 0.3727 kJ/mol, respectively. The lone pair electrons

Table 3. The NLO measurements of ICINH

Parameters	B3LYP/6-311++G(d,p)
Dipole moment (μ)	**Debye**
μ_x	1.6403
μ_y	0.4934
μ_z	0.1242
M	1.7174**Debye**
Polarizability (α_0)	***x10^{-30}esu***
α_{xx}	351.00
α_{xy}	-4.96
α_{yy}	194.94
α_{xz}	1.53
α_{yz}	4.90
α_{zz}	132.91
$\boldsymbol{\alpha_o}$	0.5902x10^{-30}esu
Hyperpolarizability (β_0)	***x10^{-30}esu***
β_{xxx}	-1163.89
β_{xxy}	31.69
β_{xyy}	148.04
β_{yyy}	-106.30
β_{xxz}	-196.67
β_{xyz}	-19.08
β_{yyz}	12.83
β_{xzz}	46.85
β_{yzz}	-42.47
β_{zzz}	-35.40
$\boldsymbol{\beta_0}$	8.6424x10^{-30}esu

Standard value for urea (**μ**=1.3732 Debye, $\boldsymbol{\beta_0}$=0.3728x10^{-30}esu): **esu**-electrostatic unit

Table 4. The Second order perturbation theory analysis of Fock Matrix in NBO basis for ICINH

Type	Donor NBO (i)	ED/e	Acceptor NBO (j)	ED/e	$^{a}E^{(2)}$ KJ/mol	$^{b}E(j)-E(i)$ a.u.	$^{c}F(i,j)$ a.u.
σ -σ*	BD (1) C 1 - C 2	1.959	BD*(1) C 1 - C 6	0.021	18.95	1.23	0.07
			BD*(1) C 2 - C 3	0.022	14.06	1.24	0.06
			BD*(1) C 2 - C 8	0.027	8.20	1.16	0.04
			BD*(1) C 3 - H 9	0.014	10.59	1.11	0.05
			BD*(1) C 6 - H 12	0.013	9.41	1.10	0.05
			BD*(1) C 8 - C 16	0.036	17.95	1.15	0.06
			BD*(1) H 13 - N 15	0.016	16.82	1.04	0.06
π -π*	BD (2) C 1 - C 2	1.596	BD*(2) C 3 - C 4	0.301	79.16	0.29	0.07
			BD*(2) C 5 - C 6	0.319	76.11	0.28	0.07
			BD*(2) C 7 - C 8	0.349	78.70	0.26	0.06
σ -σ*	BD (1) C 1 - C 6	1.976	BD*(1) C 1 - C 2	0.027	20.21	1.25	0.07
			BD*(1) C 1 - N 15	0.027	8.91	1.15	0.04
			BD*(1) C 2 - C 8	0.027	5.86	1.21	0.04
			BD*(1) C 5 - C 6	0.013	11.59	1.30	0.05
			BD*(1) C 5 - H 11	0.012	9.46	1.16	0.05
			BD*(1) C 6 - H 12	0.014	4.18	1.14	0.03
			BD*(1) C 7 - N 15	0.013	6.53	1.15	0.04
σ -σ*	BD (1) C 1 - N 15	1.986	BD*(1) C 1 - C 2	0.027	4.44	1.36	0.03
			BD*(1) C 1 - C 6	0.021	8.54	1.38	0.05
			BD*(1) C 2 - C 3	0.022	9.87	1.38	0.05
			BD*(1) C 7 - H 14	0.012	9.12	1.23	0.05
			BD*(1) C 7 - N 15	0.013	6.40	1.26	0.04
σ -σ*	BD (1) C 2 - C 3	1.974	BD*(1) C 1 - C 2	0.027	15.44	1.24	0.06
			BD*(1) C 1 - N 15	0.027	7.11	1.13	0.04
			BD*(1) C 2 - C 8	0.027	18.79	1.19	0.07
			BD*(1) C 3 - C 4	0.014	12.47	1.29	0.06
			BD*(1) C 4 - H 10	0.013	9.33	1.15	0.05
σ -σ*	BD (1) C 2 - C 8	1.962	BD*(1) C 1 - C 2	0.027	8.37	1.20	0.04
			BD*(1) C 1 - C 6	0.021	15.82	1.22	0.06
			BD*(1) C 1 - N 15	0.026	4.18	1.09	0.03

Table 4 continued from page 22

Type	Donor NBO (i)	ED/e	Acceptor NBO (j)	ED/e	$^{a}E^{(2)}$ KJ/mol	$^{b}E(j)-E(i)$ a.u.	$^{c}F(i,j)$ a.u.
			BD*(1) C 2 - C 3	0.022	16.48	1.22	0.06
			BD*(1) C 3 - C 4	0.013	5.10	1.25	0.04
			BD*(1) C 7 - C 8	0.019	12.84	1.21	0.06
			BD*(1) C 7 - H 14	0.012	18.95	1.07	0.06
			BD*(1) C 7 - N 15	0.013	5.44	1.09	0.03
			BD*(1) C 8 - C 16	0.036	10.08	1.13	0.05
			BD*(1) C 16 - N 18	0.010	9.50	1.25	0.05
σ -σ*	BD (1) C 3 - C 4	1.978	BD*(1) C 2 - C 3	0.023	13.77	1.27	0.06
			BD*(1) C 2 - C 8	0.027	19.25	1.19	0.07
			BD*(1) C 3 - H 9	0.014	4.69	1.14	0.03
			BD*(1) C 4 - C 5	0.016	10.84	1.26	0.05
			BD*(1) C 5 - H 11	0.012	8.49	1.15	0.04
π -π*	BD (2) C 3 - C 4	1.721	BD*(2) C 1 - C 2	0.477	75.10	0.28	0.07
			BD*(2) C 5 - C 6	0.319	82.34	0.28	0.07
σ -σ*	BD (1) C 3 - H 9	1.979	BD*(1) C 1 - C 2	0.027	17.24	1.06	0.06
			BD*(1) C 4 - C 5	0.016	16.07	1.08	0.06
σ -σ*	BD (1) C 4 - C 5	1.979	BD*(1) C 3 - C 4	0.013	11.17	1.28	0.05
			BD*(1) C 3 - H 9	0.014	10.46	1.13	0.05
			BD*(1) C 5 - C 6	0.013	10.92	1.27	0.05
			BD*(1) C 6 - H 12	0.013	11.05	1.12	0.05
σ -σ*	BD (1) C 4 - H 10	1.980	BD*(1) C 2 - C 3	0.022	15.98	1.08	0.06
			BD*(1) C 5 - C 6	0.013	15.94	1.10	0.06
σ -σ*	BD (1) C 5 - C 6	1.976	BD*(1) C 1 - C 6	0.021	13.97	1.27	0.06
			BD*(1) C 1 - N 15	0.026	25.98	1.14	0.08
			BD*(1) C 4 - C 5	0.015	10.54	1.27	0.05
			BD*(1) C 4 - H 10	0.012	8.28	1.15	0.04
			BD*(1) C 6 - H 12	0.013	5.27	1.13	0.03
π -π*	BD (2) C 5 - C 6	1.729	BD*(2) C 1 - C 2	0.477	82.01	0.28	0.07
			BD*(2) C 3 - C 4	0.301	72.63	0.29	0.06
σ -σ*	BD (1) C 5 - H 11	1.980	BD*(1) C 1 - C 6	0.022	14.69	1.08	0.06
			BD*(1) C 3 - C 4	0.0140	15.69	1.11	0.06
σ -σ*	BD (1) C 6 - H 12	1.980	BD*(1) C 1 - C 2	0.027	17.66	1.07	0.06
			BD*(1) C 4 - C 5	0.016	15.06	1.09	0.06

OPEN ACCESS
Freely Available Online

Table 4 continued from page 23

Type	Donor NBO (i)	ED/e	Acceptor NBO (j)	ED/e	$^{a}E^{(2)}$ KJ/mol	$^{b}E(j)-E(i)$ a.u.	$^{c}F(i,j)$ a.u.
σ -σ*	BD (1) C 7 - C 8	1.972	BD*(1) C 2 - C 3	0.023	20.42	1.28	0.07
			BD*(1) C 2 - C 8	0.027	12.18	1.21	0.05
			BD*(1) C 7 - H 14	0.012	6.53	1.13	0.04
			BD*(1) C 8 - C 16	0.036	12.34	1.20	0.05
			BD*(1) H 13 - N 15	0.017	14.02	1.09	0.05
			BD*(1) C 16 - H 17	0.022	4.23	1.13	0.03
π -π*	BD (2) C 7 - C 8	1.801	BD*(2) C 1 - C 2	0.477	66.23	0.30	0.07
			BD*(2) C 7 - C 8	0.349	8.87	0.29	0.02
			BD*(2) C 16 - N 18	0.212	73.60	0.29	0.06
σ -σ*	BD (1) C 7 - H 14	1.984	BD*(1) C 1 - N 15	0.026	12.26	1.01	0.05
			BD*(1) C 2 - C 8	0.027	8.66	1.06	0.04
			BD*(1) C 7 - C 8	0.019	6.07	1.13	0.04
σ -σ*	BD (1) C 7 - N 15	1.985	BD*(1) C 1 - C 6	0.021	17.03	1.39	0.07
			BD*(1) C 1 - N 15	0.026	7.32	1.26	0.04
			BD*(1) C 7 - C 8	0.019	5.06	1.38	0.04
			BD*(1) C 8 - C 16	0.036	16.07	1.30	0.06
σ -σ*	BD (1) C 8 - C 16	1.979	BD*(1) C 1 - C 2	0.027	4.81	1.23	0.03
			BD*(1) C 2 - C 8	0.027	14.31	1.18	0.06
			BD*(1) C 7 - C 8	0.019	14.81	1.24	0.06
			BD*(1) C 7 - N 15	0.013	4.48	1.13	0.03
			BD*(1) C 16 - N 18	0.010	9.54	1.29	0.05
σ -σ*	BD (1) H 13 - N 15	1.990	BD*(1) C 1 - C 2	0.027	7.41	1.24	0.04
			BD*(1) C 7 - C 8	0.019	5.73	1.26	0.04
σ -σ*	BD (1) C 16 - H 17	1.969	BD*(1) C 7 - C 8	0.019	20.08	1.07	0.06
			BD*(1) N 18 - N 19	0.030	35.31	0.89	0.08
σ -σ*	BD (1) C 16 - N 18	1.988	BD*(1) C 2 - C 8	0.027	4.98	1.39	0.04
			BD*(1) C 8 - C 16	0.036	9.37	1.38	0.05
			BD*(1) N 19 - C 21	0.073	10.33	1.33	0.05
π -π*	BD (2) C 16 - N 18	1.942	BD*(2) C 7 - C 8	0.349	32.55	0.35	0.05
σ -σ*	BD (1) N 18 - N 19	1.986	BD*(1) C 16 - H 17	0.022	8.62	1.27	0.05
			BD*(1) C 21 - O 29	0.021	5.69	1.44	0.04
σ -σ*	BD (1) N 19 - H 20	1.983	BD*(1) C 21 - C 22	0.066	15.10	1.09	0.06
σ -σ*	BD (1) N 19 - C 21	1.990	BD*(1) C 16 - N 18	0.010	8.91	1.42	0.05
			BD*(1) C 22 - C 23	0.021	4.39	1.39	0.03
			BD*(1) C 25 - C 23	0.026	4.23	4.67	0.06

OPEN ACCESS
Freely Available Online

Table 4 continued from page 24

Type	Donor NBO (i)	ED/e	Acceptor NBO (j)	ED/e	$^{a}E^{(2)}$ KJ/mol	$^{b}E(j)-E(i)$ a.u.	$^{c}F(i,j)$ a.u.
σ -σ*	BD (1) C 21 - C 22	1.974	BD*(1) N 19 - H 20	0.042	10.96	1.03	0.05
			BD*(1) C 21 - O 29	0.021	5.27	1.24	0.04
			BD*(1) C 22 - C 23	0.021	7.07	1.23	0.04
			BD*(1) C 22 - C 24	0.033	8.12	1.22	0.04
			BD*(1) C 23 - C 25	0.015	9.08	1.25	0.05
			BD*(1) C 25 - N 32	0.015	9.50	1.21	0.05
σ -σ*	BD (1) C 21 - O 29	1.992	BD*(1) N 18 - N 19	0.030	7.28	1.39	0.04
			BD*(1) C 21 - C 22	0.066	7.11	1.45	0.05
			BD*(1) C 22 - C 24	0.033	5.61	1.59	0.04
π -π*	BD (2) C 21 - O 29	1.979	BD*(2) C 22 - C 24	0.328	13.85	0.42	0.04
σ -σ*	BD (1) C 22 - C 23	1.973	BD*(1) N 19 - C 21	0.073	8.49	1.13	0.04
			BD*(1) C 21 - C 22	0.066	7.07	1.12	0.04
			BD*(1) C 22 - C 24	0.033	14.85	1.26	0.06
			BD*(1) C 23 - C 25	0.0148	10.84	1.29	0.05
			BD*(1) C 24 - H 27	0.023	9.50	1.15	0.05
			BD*(1) C 25 - H 28	0.013	10.59	1.14	0.05
σ -σ*	BD (1) C 22 - C 24	1.979	BD*(1) C 21 - C 22	0.066	6.23	1.13	0.04
			BD*(1) C 21 - O 29	0.021	6.65	1.29	0.04
			BD*(1) C 22 - C 23	0.021	16.07	1.27	0.06
			BD*(1) C 23 - H 26	0.014	10.42	1.16	0.05
			BD*(1) C 24 - H 27	0.023	4.35	1.15	0.03
			BD*(1) C 24 - C 30	0.015	5.90	1.26	0.04
π -π*	BD (2) C 22 - C 24	1.610	BD*(2) C 21 - O 29	0.274	74.39	0.29	0.07
			BD*(2) C 23 - C 25	0.287	97.53	0.28	0.07
			BD*(2) C 28 - N 31	0.372	68.03	0.27	0.06
σ -σ*	BD (1) C 23 - C 25	1.979	BD*(1) C 21 - C 22	0.066	12.01	1.13	0.05
			BD*(1) C 22 - C 23	0.021	12.22	1.27	0.05
			BD*(1) C 25 - H 28	0.014	4.35	1.15	0.03
			BD*(1) C 30 - H 31	0.024	9.25	1.14	0.05
π -π*	BD (2) C 23 - C 25	1.639	BD*(2) C 22 - C 24	0.329	69.33	0.29	0.06
			BD*(2) C 30 - N 32	0.373	123.22	0.27	0.08
σ -σ*	BD (1) C 23 - H 26	1.979	BD*(1) C 22 - C 24	0.033	16.99	1.08	0.06
σ -σ*	BD (1) C 24 - H 27	1.979	BD*(1) C 22 - C 23	0.021	17.45	1.08	0.06
			BD*(1) C 30 - N 32	0.016	20.33	1.06	0.06

OPEN ACCESS
Freely Available Online

OpenAccessPub

Table 4 continued from page 25

Type	Donor NBO (i)	ED/e	Acceptor NBO (j)	ED/e	[a]E(2) KJ/mol	[b]E(j)-E(i) a.u.	[c]F(i,j) a.u.
σ -σ*	BD (1) C 24 - N 31	1.986	BD*(1) C 21 - C 22	0.066	9.41	1.25	0.05
			BD*(1) C 22 - C 24	0.033	8.12	1.38	0.05
			BD*(1) C 28 - H 30	0.024	8.74	1.25	0.05
σ -σ*	BD (1) C 25 - C 23	1.985	BD*(1) C 23 - C 25	0.015	10.59	1.30	0.05
			BD*(1) C 23 - H 26	0.014	11.63	1.16	0.05
			BD*(1) C 30 - N 32	0.016	5.86	1.26	0.04
σ -σ*	BD (1) C 25 - H 23	1.979	BD*(1) C 22 - C 23	0.021	14.52	1.09	0.06
			BD*(1) C 30 - N 32	0.016	17.87	1.07	0.06
σ -σ*	BD (1) C 30 - H 31	1.982	BD*(1) C 23 - C 25	0.015	14.73	1.11	0.06
			BD*(1) C 25 - N 32	0.015	20.17	1.07	0.06
σ -σ*	BD (1) C 30 - N 32	1.987	BD*(1) C 24 - H 27	0.023	8.79	1.27	0.05
			BD*(1) C 25 - H 29	0.013	6.11	1.26	0.04
π -π*	BD (2) C 30 - N 32	1.705	BD*(2) C 22 - C 24	0.328	116.40	0.32	0.09
			BD*(2) C 23 - C 25	0.287	52.38	0.32	0.06
n -π*	LP (1) N 15	1.613	BD*(2) C 1 - C 2	0.476	140.71	0.30	0.09
			BD*(2) C 7 - C 8	0.349	160.41	0.29	0.10
n -σ*	LP (1) N 18	1.921	BD*(1) C 8 - C 16	0.036	42.76	0.87	0.09
			BD*(1) C 16 - H 17	0.022	16.74	0.80	0.05
			BD*(1) N 19 - H 20	0.042	33.05	0.75	0.07
n -π*	LP (1) N 19	1.679	BD*(2) C 16 - N 18	0.212	102.42	0.30	0.08
			BD*(1) C 21 - O 29	0.021	5.40	0.87	0.03
			BD*(2) C 21 - O 29	0.274	170.41	0.33	0.10
n -σ*	LP (1) N 32	1.917	BD*(1) C 22 - C 24	0.033	39.46	0.89	0.08
			BD*(1) C 24 - H 27	0.023	16.57	0.78	0.05
			BD*(1) C 25 - C 23	0.026	8.16	4.18	0.08
			BD*(1) C 30 - H 31	0.023	17.11	0.77	0.05
n -σ*	LP (1) O 29	1.979	BD*(1) C 21 - C 22	0.066	8.24	1.12	0.04
n -σ*	LP (2) O 29	1.868	BD*(1) N 19 - C 21	0.073	99.66	0.68	0.12
			BD*(1) C 21 - C 22	0.066	73.35	0.68	0.10
			BD*(1) C 25 - C 23	0.026	6.90	4.10	0.08
π*-π*	BD*(2) C 1 - C 2	0.477	BD*(2) C 3 - C 4	0.301	1195.8	0.01	0.08
π*-π*	BD*(2) C 7 - C 8	0.349	BD*(2) C 1 - C 2	0.477	711.11	0.01	0.06
π*-σ*	BD*(2) C 21 - O 29	0.274	BD*(1) C 21 - O 29	0.021	18.24	0.54	0.11
π*-π*	BD*(2) C 30 - N 32	0.373	BD*(2) C 22 - C 24	0.328	604.96	0.02	0.08
			BD*(2) C 23 - C 25	0.287	714.04	0.02	0.08

[a] $E^{(2)}$ means energy of hyper conjugative interaction (stabilization energy).
[b] Energy difference between donor (i) and acceptor (j) nbo orbitals.
[c] F(i,j) is the Fock matrix element between i and j nbo orbitals.

www.openaccesspub.org | JNDC CC-license DOI : 10.14302/issn.2377-2549.jndc-17-1459 Vol-1 Issue –3 Page No– 26

are readily available for the interaction with excited electrons of antibonding orbital. During n-π* transition, more energy delocalization takes place: N_{19}→C_{16}-N_{18}; C_{21}→O_{29} and N_{15}→C_1-C_2; C_7-C_8. The corresponding excitation energy values are, 102.42, 170.41 and 140.71, 160.41, respectively. In which, these (N_{19}→C_{21}-O_{29} & N_{15}→C_7-C_8) two transitions give the strongest stabilization to the system.

HOMO–LUMO Analysis

The HOMO–LUMO plot of ICINH molecule is shown in Fig. 4 In HOMO diagram, the colored portions indicate the prominent donor levels which contribute in the electronic transitions and similarly the LUMO diagram indicates the prominent acceptors level through colored shades which involve in the electronic transitions. Homo localized in the indole and carbonyl group. The LUMO is located over the pyridine and hydrazone linkage. The molecule ICINH has lower energy gap and hence the probability of π-π* proton transition is highly possible in between HOMO and LUMO orbitals. The HOMO/LUMO energies are calculated using B3LYP/6-311++G(d,p) level.

By using HOMO and LUMO energy value ICINH, the global chemical reactivity descriptors such as hardness (η), chemical potential (μ), softness (S), electronegativity (χ) and electrophilicity index (ω) have been calculated and are listed in Table 5. It can be expressed through HOMO and LUMO orbital energies as $I=-E_{HOMO}$ and $A=-E_{LOMO}$, the electron affinity I and Ionization potential A of title molecule ICINH are also calculated by using B3LYP/6-311++G(d,p) basis set. The calculated values of the softness, hardness, chemical potential electronegativity and electrophilicity index, Homo, Lumo and energy gap of the molecule are: 4.341 eV, 3.954 eV, 3.954 eV and 1.801 eV, -6.125 eV, -1.784 eV and 4.341 eV, respectively. The soft molecule has small energy gap and hard molecule has large energy gap. In addition, the frontier molecular orbital energies are also calculated using the same basis set and are listed in Table 6.

UV-Vis Spectra

The UV absorption spectrum for ICINH is recorded in the range 200-800 nm. All the structures allow strong π-π* and σ-σ* transition in the UV-Vis region with high extinction coefficients. The calculated results involving in the vertical excitation energies, oscillator strength (f) and wavelength are carried out and compare with measured experimental wavelength. Typically, according to Frank-Condon principle, the maximum absorption peaks (λ_{max}) in a UV-Vis spectrum correspond to vertical excitation. The λ_{max} of ICINH molecule are calculated using TD-DFT/6-311++G(d,p) basis set. It is evident from the Table 7, the possible π-π* transitions, with absorption maximum at 413.14, 389.2, 357.32 nm, belong to gas phase and the oscillator strength for respective transitions are 0.0009, 0.0136 and 0.0296, respectively. The calculated absorption maxima has been found to be 357.32 nm which is moderately coincides with the experimental value 342.42 nm. The combined theoretical and experimental UV-Vis absorption spectra are shown in Fig. 5.

Molecular electrostatic potential

In the present study, MEP surface map of ICINH is calculated using B3LYP/6-311++G(d,p) basis set and illustrated in Fig. 6 The MEP which is a plot of electrostatic potential map onto the constant ED surface. In the majority of the MEPs, the maximum negative region which is the preferred site for electrophilic attack and the maximum positive region is the preferred site for nucleophilic attack. The importance of MEPs lies in the fact that it simultaneously displays molecular size, shape as well as positive, negative and neutral electrostatic potential regions in terms of colour scheme (Fig. 6) and is very useful in research of molecular

HOMO = -6.126 eV

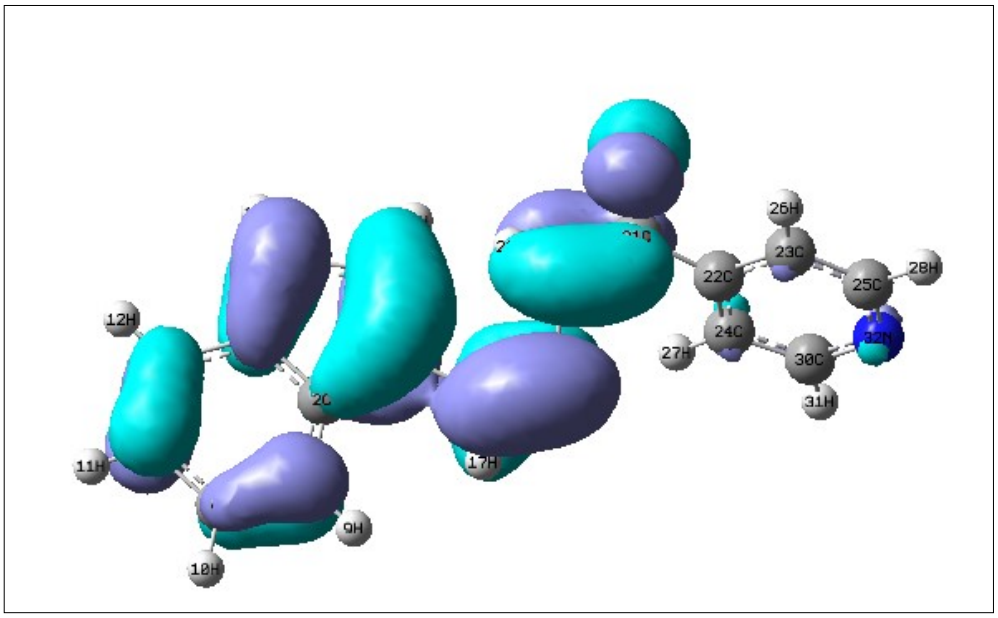

Energy gap = 4.341 eV

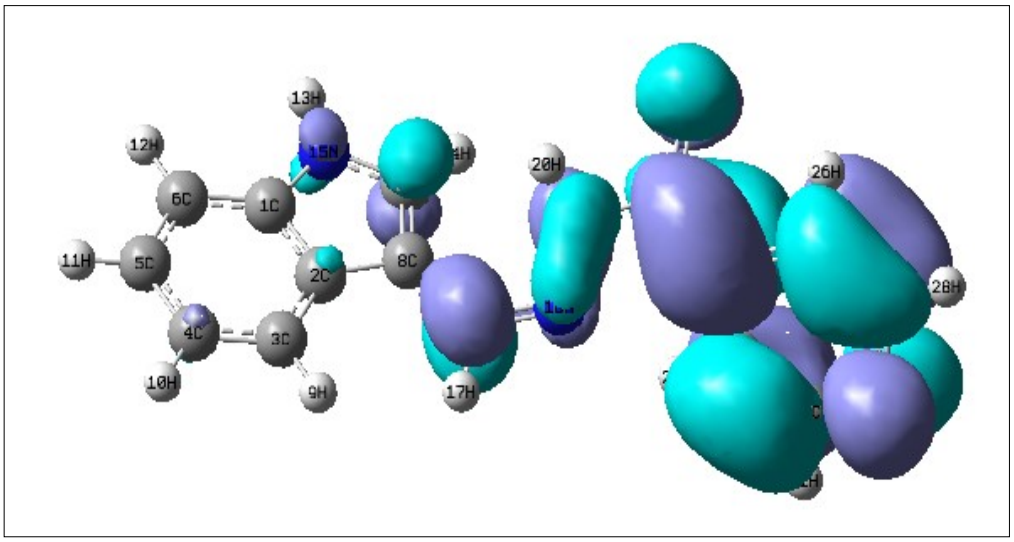

Lumo = -1.784 eV

Fig. 4. The frontier molecular orbitals of ICINH

Table 5. The Physico-chemical properties of ICINH

Parameters	Values
HOMO	-6.125 eV
LUMO	-1.784 eV
Energy gap	4.341 eV
Ionization potential (IP)	6.125 eV
Electron affinity (EA)	1.784 eV
Electrophilicity Index (ω)	1.801
Chemical Potential (μ)	3.954
Electronegativity (χ)	-3.954
Hardness (η)	-4.341
Softness (S)	8.682

Table 6. The frontier molecular orbitals of ICINH

Occupancy	Orbital energies (a.u)	Orbital energies (eV)	Kinetic energies (a.u)
O_{52}	-0.269	-7.319	1.267
O_{53}	-0.267	-7.265	1.605
O_{54}	-0.262	-7.129	1.871
O_{55}	-0.254	-6. 911	1.250
O_{56}	-0.228	-6.203	1.576
V_{57}	-0.071	-1.931	1.664
V_{58}	-0.055	-1.496	1.519
V_{59}	-0.034	0. 925	1.367
V_{60}	0.025	0.680	0.381
V_{61}	0.023	0.625	1.250

Table 7. The electronic transition of ICINH

Calculated at B3LYP/ 6-311++G (d,p)	Oscillator strength	Calculated Band gap (ev/nm)	Experimental Band gap (ev/ nm)	Type
Excited State-1	Singlet-A (f=0.0009)	3.0010 eV/413.14 nm		
69 -> 70	0.6908			
Excited State-2	Singlet-A (f=0.0136)	3.1849 eV/389.29 nm		
66 -> 70	-0.1059			
68 -> 70	0.6587			
68 -> 71	0.1308			
Excited State-3	Singlet-A (f=0.0296)	3.4698 eV/357.32 nm	342.42	**π-π***
66 -> 70	0.1243			
66 -> 71	0.1564			
68 -> 70	-0.1275			
68 -> 71	0.4689			
69 -> 71	-0.4067			

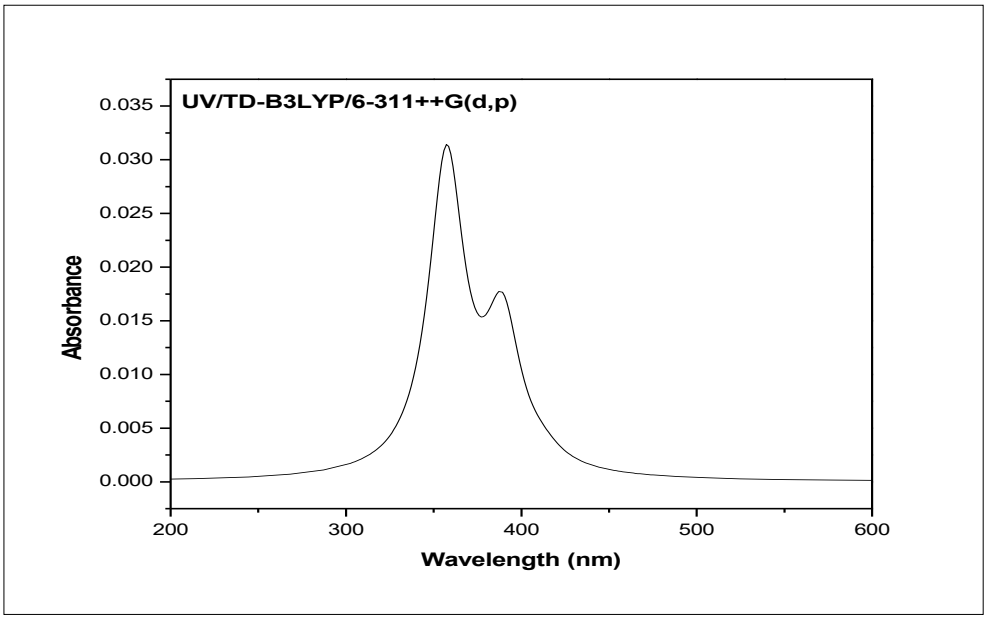

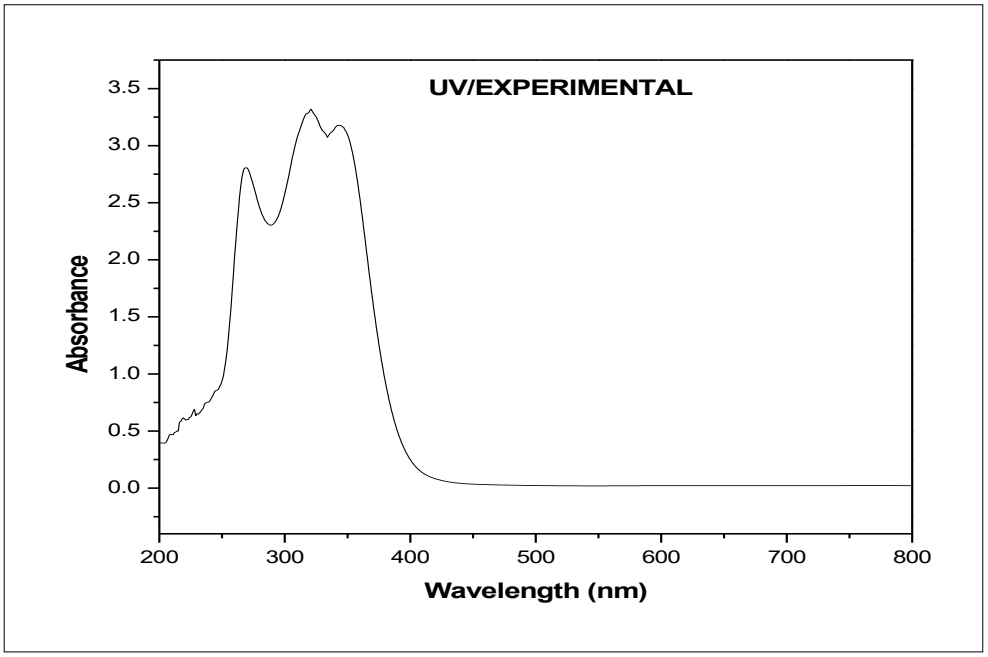

Fig. 5. The combined theoretical and experimental UV-Visible spectra of ICINH

structure with its physiochemical property relationship [26,27]. The color scheme for the MEP surface is as follows: red for electron rich, partially negative charge: blue correspond to electron deficient, partially positive charge: green for neutral, respectively [28,29]. The electrostatic potential increases in the order of red< orange<yellow<green<blue. The color code of the map range between -9.185 e^{-2} (deepest red) to 9.185 e^{-2} (deepest blue). It is seen from the MEP map of the title molecule, the regions having the negative potential over the electronegative atom (oxygen atom), and the regions having the positive potential over all the hydrogen atoms in indole ring. The oxygen atom indicates the strong repulsion with other atom. These two ends of the molecule which are positively and negatively charged are prone to electrophilic and electrophobic reactions with other molecules.

Mulliken Atomic Charges

It is well known that the atomic charges are very much dependent on how the atoms are defined. It also plays an important role in the application of quantum chemical calculation to molecular system because of atomic charges affect the dipole moment, molecular polarizability, electronic structure and a lot of properties of molecular systems. The mulliken charges calculated at B3LYP/6-311++G(d,p) basis set for the molecule under study are given in Table 8. The mulliken atomic charges plot for ICINH is shown in Fig. 7 The C_2 atom has high positive charge which is due to the indole group. Similarly the C_{16} atom has high negative charge due to the attachment of C_{16}=N_{18} group. All the hydrogen atoms have positive charge.

Thermodynamic Properties

On the basis of vibrational analysis, the standard statistical thermodynamic functions: heat capacity (C), entropy (S) and enthalpy changes (H) for the title molecule are obtained from the theoretical harmonic frequencies and are listed in Table 9. From Table 10, it can be observed that these thermodynamic functions are increasing with temperature ranging from 100 to 1000 K. The obvious reason for this is almost linear increase, and this is due to the increase in internal energy of the molecule in accordance with kinetic theory of gases due to the fact that the molecular vibrational intensities increase with temperature [30]. The correlation equations between heat capacities, entropies, enthalpy, changes and temperatures are fitted by quadratic formulas and the corresponding fitting factors (R^2) for these thermodynamic properties are 0.99905, 0.9994 and 0.99998, respectively and the correlation graphics are shown in Fig. 8.

They can be used to compute the other thermodynamic energies according to relationships of thermodynamic functions and estimate directions of chemical reactions according to the second law of thermodynamics in thermo chemical field [31]. In this study all thermodynamic calculations are done in gas phase and they could not be used in solution.

$C^0_{p,m}$ = 6.76926 + 0.02858T + 2.52495x10^{-5} T^2 (R^2 = 0.99905)

S^0_m = 1.40875 + 0.00595T + 5.25468x10^{-5} T^2 (R^2 = 0.99998)

ΔH^0_m = 4.06057 + 0.01714T + 1.51461x10^{-5} T^2 (R^2 = 0.9994)

Conclusion

The FT-IR, FT-Raman and UV-Vis spectra of the compound ICINH had been recorded and analyzed. The detailed interpretations of the vibrational spectra had been carried out. The optimized geometrical parameters were calculated and compared with the reported XRD data. The vibrational assignments were further justified with help of the PED analysis. The HOMO-LUMO energy gap indicated the stability and reactivity of the title

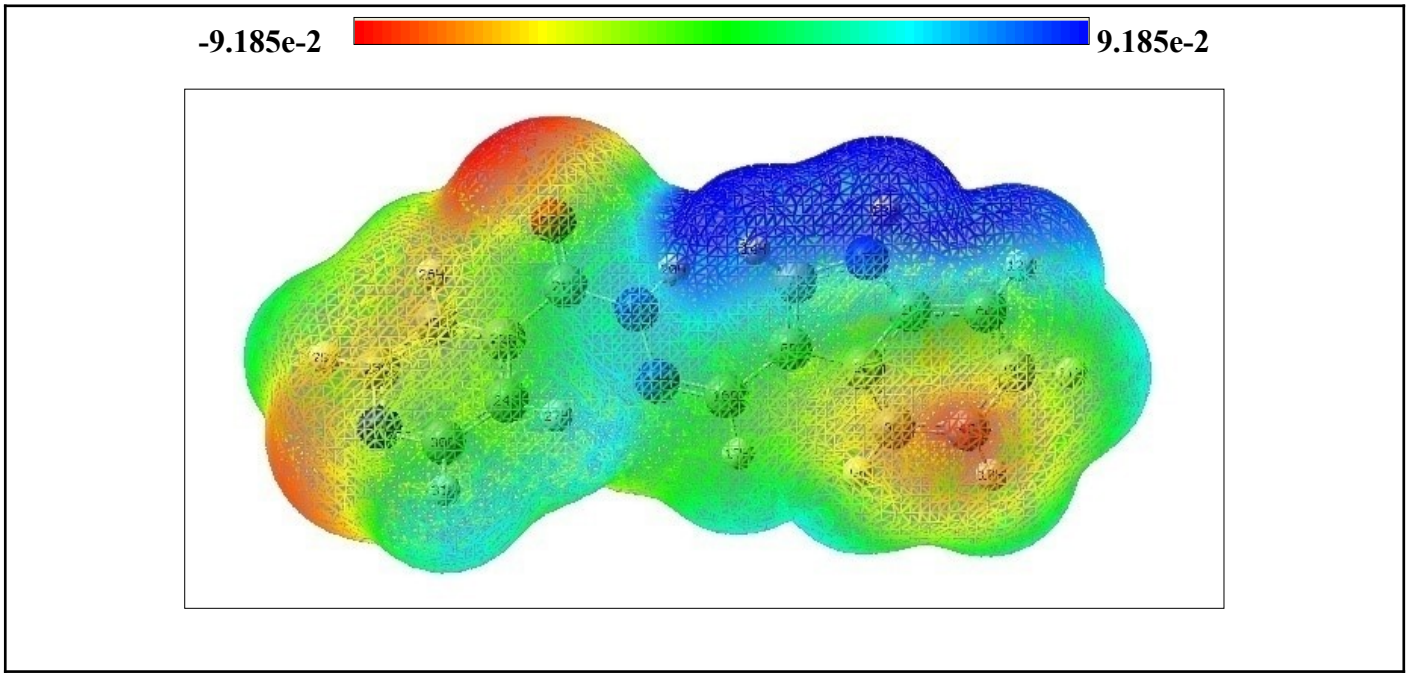

Fig. 6. The molecular electrostatic potential map of ICINH

Table 8. The Mulliken atomic charges of ICINH

Atoms	Charges	Atoms	Charges
1C	-0.2987	17H	0.1624
2C	1.3144	18N	0.0896
3C	-0.6692	19N	-0.0922
4C	-0.5107	20H	0.2843
5C	-0.0917	21C	-0.5353
6C	-0.6358	22C	0.7243
7C	-0.2138	23C	0.0949
8C	0.8639	24C	-0.5605
9H	0.1424	25C	-0.1468
10H	0.1605	26H	0.2244
11H	0.1674	27H	0.2180
12H	0.1439	28C	-0.2971
13H	0.3039	29H	0.1812
14H	0.2100	30H	0.1860
15N	-0.0449	31N	-0.0054
16C	-1.1123	32O	-0.2591

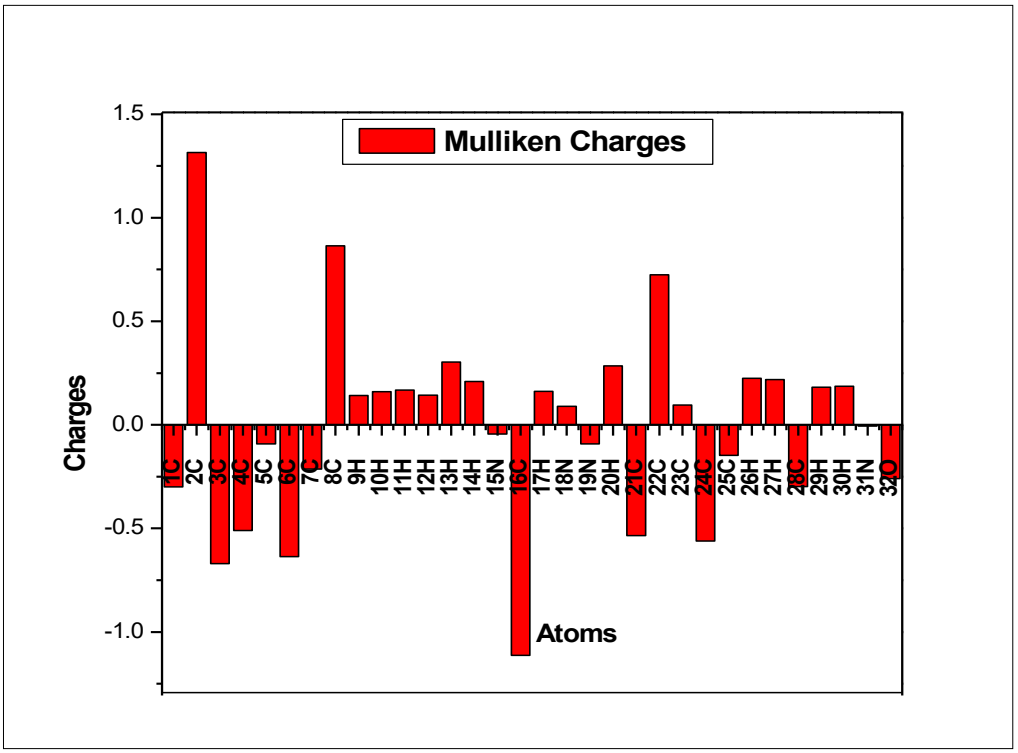

Fig. 7. The Mulliken atomic charges of ICINH

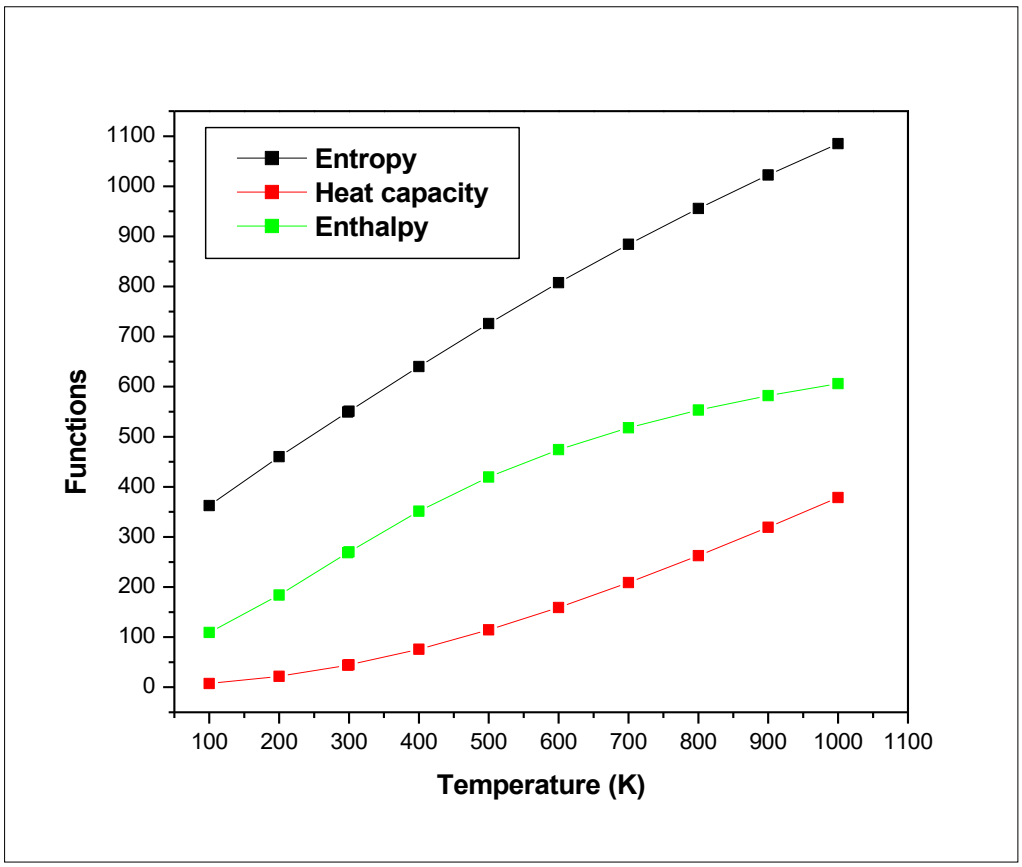

Fig. 8. The thermodynamic properties of ICINH at different temperatures

Table 9. The calculated total energy (a.u), zero point vibrational energies (Kcal/mol), rotational constants (GHz) and entropy (cal/mol K^{-1}) for ICINH

Parameters	B3LYP/6-311++G(d,p)
Total Energies	-873.259
Zero-point Energy	154. 930 (Kcal/Mol)
Rotational constants (GHZ)	1.119
	0.128
	0.120
Entropy	
Total	131.409
Translational	42.613
Rotational	34.185
Vibrational	54.610

Table 10. Thermodynamic Properties of ICINH at different temperatures

T (K)	S (J/mol.K)	Cp (J/mol.K)	ddH (kJ/mol)
100.00	362.62	109.42	7.39
200.00	460.26	183.91	21.90
298.15	549.35	268.44	44.07
300.00	551.01	270.03	44.57
400.00	640.10	351.39	75.73
500.00	726.10	419.62	114.40
600.00	807.63	474.29	159.20
700.00	884.14	517.90	208.89
800.00	955.68	553.15	262.50
900.00	1022.55	582.09	319.31
1000.00	1085.17	606.19	378.76

compound. The good correlation between the UV-Vis, absorption maxima and calculated electronic absorption maxima were found. The donor-acceptor interaction, as obtained from NBO analysis could fairly explains the decrease of occupancies of σ bonding orbital and the increase of occupancy of π* anti-bonding orbitals. In addition, mulliken atomic charges, MEP, Thermodynamic parameters, first order hyperpolarizabilities and dipole moment of the title compound were also calculated.

References

1. H. Ozisik, S. Saglam, S.H. Bayari, Sturct. Chem. 19 (2009) 41–50.
2. J.V. Hidgon, B.W. Delage, R.H. Dashwood, Pharmacol. Res. 55 (3) (2007) 224.
3. F. Billes, P.V. Podea, I. Mohammed-Ziegler, M. Tosa, H. Mikosch, D.F. Irimie, Spectrochim. Acta A 74 (2009) 1031–1045.
4. L. Taiz, E. Zeiger, Plant Physiology, second ed., Sinauer Associates, Inc., Massachusetts,1998.
5. J.R. Carney, S.Z. Timothy, J. Phys. Chem. A 104 (2004) 8677–8688.
6. V. Vasantha Kumar, S.L. Gouda, J. Laxmikanth Rao, Ab initioand density functional theory studies on vibrational spectra of 3-hydroxy-3-(2-methyl-1H-indol-3-yl)indolin-2-one, Spectrochimica Acta Part A: Molecular and Biomolecular Spectroscopy 103 (2013) 304–310.
7. H. Saleem, S. Subashchandrabose, Y. Erdogduc, V. Thanikachalam, J. Jayabharathi, FT-IR, FT-Raman spectral and conformational studies on (E)-2-(2-hydroxybenzylidenamino)-3-(1H-indol-3yl) propionic acid, Spectrochimica Acta Part A: Molecular and Biomolecular Spectroscopy 101 (2013) 91–99.
8. N. Ramesh Babu, S. Subashchandrabose, M. Syed Ali Padusha, H. Saleem, V. Manivannan, Y. Erdog˘du, Synthesis and structural characterization of (E)-N0-((Pyridin-2-yl)methylene) benzohydrazide by X-ray diffraction, FT-IR, FT-Raman and DFT methods, Journal of Molecular Structure 1072 (2014) 84–93.
9. P. Lissoni, R. Bucovec, A. Bonfonti, L. Giani, A. Mandelli, M. G. Roselli, F. Rovelli, L. Fumapalli, J. Pineal Res. 30 (2) (2001) 123. 15. R. G. Parr, W. Yang, Density Functional Theory of Atoms and molecules, Oxford, New York, 1989.
10. R. O. Jones, O. Gunnarson, Rev. Mod. Phys. 61 (1989) 689-746.
11. T. Ziegler, Chem. Rev. 91 (1991) 651-667.
12. W. Kohn, L. J. Sham, Phys. Rev.146 (1965) A1133-A1138.
13. C. James, G. R. Pettit, O. F. Nielsen, V. S. Jayakumar, T. H. Joe, Spectrochimm. Acta A 70 (2008) 1208-1216.
14. Babu, Dickson., Gachumale, S., Sambandam, A., Airody Vasudeva, A., New D-p-A Type indole based chromoogens for DSSC: Design Synthesis and Performance studies', Dyes and Pig.112 (2015) 183-191.
15. Hassan, M., Badawi, Former, W. "analysis of the molecular Stutucture and vibrational spectra of the title indole based analgesic drug indomethacin", Spectrochim. Acta A: Mol. Biomol. Spectrosc. 123 2014) 447-454.
16. R. Bikas, F. Sattarri, B. Notash, Acta Cryst. E 68 (2012) M132-M133.
17. Rauhut, G., Pulay, P., Transferable Scaling Factors for Density Functional Derived Vibrational Force Fields, J.Phys.Chem. 99 (1995) 3093-3100.
18. V. Krishnakumar, R. Ramasamy, Indian J Pure & Appl. Phys., 40 (2002) 252.
19. George W.O. & Mcintyre P.S, Infrared Spectroscopy, John Wiley & Sons, London, (1987).
20. Bellamy L.J, The infrared spectra of complex molecules, John Wiley, New York, (1959).
21. Mehmet Karabacak, J. Mol. Struct. 919 (2009) 215–222.
22. M. Silverstein, G. Clayton Basseler, C. Morill, Spectrometric Identification of Organic Compounds, Wiley, New York, 1981.

23. S. Ramalingam, S. Periandy, B. Narayanan, S. Mohan, Spectrochim. Acta A 76 (2010) 84–92.
24. A.N. Nikitina, L.P. Yakovlev, N.S. Fedotov, B.M. Mikhailov, Zhurnal Prikladnoi spektroskopii, 6(2) (1967) 232-238.
25. Y.X.Sun, Q.L.Hao, W.X.Wei, Z.X.Yu, L.D.Lu, X.Wang, Y.S.Wang J.Mol.Struct. (Therochem) 904 (2009)74.
26. J.S. Murray, K. Sen, Molecular Electrostatic Potentials, Concepts and Applications, Elsevier, Amsterdam, 1996.
27. E. Scrocco, J. Tomasi, in: P. Lowdin (Ed.) Advances in Quantum Chemistry, Academic Press, New York, 1978.
28. H.Roohi, A.R.Nowroozi, E.Anjomshoa, Compt. Theor. Chem. 965 (2011) 211-220.
29. P.Munshi, T.N.Guru Row, Acta Cryst.B 62 (2006) 612-626.
30. J.Bevan Ott, J.Boerio-Goates, Calculations from statistical thermodynamics, 588 Acasemic Press, 2000.589.
31. R.Zhang, B.Dub, G.Sun, Y.Sun, Spectrochim. Acta A 75 (2010) 1115-1124.